REVIEW

Check for updates

Catalyst design strategies for NO$_x$-involved electrocatalytic C−N coupling reactions

Ruhan Wang,[a,b] Xiaofu Sun [iD] *[a,b] and Buxing Han [iD] *[a,b]

Electrocatalytic C−N coupling reactions involving NO$_x$ species (NO$_3^-$, NO$_2^-$, and NO) have emerged as a sustainable approach for synthesizing high-value nitrogen-containing chemicals. This review provides a comprehensive overview of the recent advances in catalyst design strategies for enhancing the efficiency and selectivity of NO$_x$-involved C−N bond formation. Five key strategies are categorized and discussed: defect engineering, coordination environment design, interface engineering, dual-site synergy, and emerging architectures. Regarding each strategy, representative literature cases are summarized to illustrate mechanistic insights and practical applications. By addressing challenges such as intermediate instability, low selectivity, and competing side reactions, these strategies demonstrate great potential for advancing electrocatalytic C−N coupling toward practical implementation. Finally, future directions are proposed, including dynamic catalyst design, microenvironment regulation, and data-driven catalyst screening.

1 Introduction

In the context of accelerating the global transition toward sustainable chemistry, electrocatalysis and electrosynthesis have garnered extensive attention as green, efficient, and versatile platforms[1–3] for producing high-value chemicals under mild ambient conditions.[4–9] These processes leverage renewable electricity and water as energy sources and benign hydrogen sources, providing an efficient and clean alternative to traditional thermochemical methods.[10,11] Over the past several decades, significant advances have been made in the electrocatalytic transformation of abundant and renewable small-molecule feedstocks (such as CO$_2$, N$_2$ and NO$_3^-$) into wide energy-rich/functionalized compounds.[9,12–22] Beyond the independent transformation of individual small molecules, increasing attention has recently shifted toward electrocatalytic strategies that integrate multiple substrates (particularly nitrogen and carbon sources) into a single reaction framework.[23–31]

[a]Beijing National Laboratory for Molecular Sciences, CAS Laboratory of Colloid and Interface and Thermodynamics, CAS Research/Education Center for Excellence in Molecular Sciences, Center for Carbon Neutral Chemistry, Institute of Chemistry, Chinese Academy of Sciences, Beijing 100190, China. E-mail: sunxiaofu@iccas.ac.cn, hanbx@iccas.ac.cn
[b]School of Chemical Sciences, University of Chinese Academy of Sciences, Beijing 100049, China

Ruhan Wang obtained her B.E. from the College of Materials Science and Technology at Beijing Forestry University. Under the supervision of Prof. Xiaofu Sun from the Institute of Chemistry, Chinese Academy of Science (CAS), she embarked on her Ph.D. studies with a focus on the utilization and conversion of NO$_x$.

Ruhan Wang

Xiaofu Sun received his B.S. degree in Chemistry from Nankai University and M.S. degree in Physical Chemistry from Renmin University of China. He earned his Ph.D. degree at ICCAS, and pursued postdoctoral research at Nanyang Technological University. He has been a professor at ICCAS since 2019. His current research interest covers the utilization and conversion of CO$_2$/NO$_x$, applications of green solvents (e.g., H$_2$O and ionic liquids), and design and synthesis of novel catalysts and catalytic systems.

Xiaofu Sun

6926 | *Inorg. Chem. Front.*, 2025, **12**, 6926–6945

This journal is © the Partner Organisations 2025
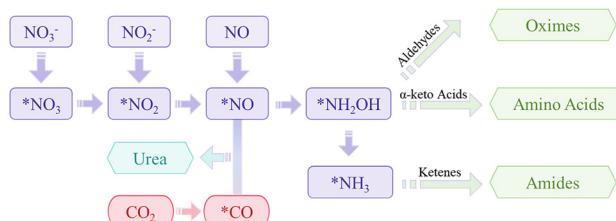
Fig. 1 Reaction pathways for NO_x-involved C–N coupling.

Electrocatalytic C–N coupling reactions, particularly those involving nitrogen oxides (NO_x, including NO, NO_2^-, and NO_3^-),[32–36] have emerged as a transformative research frontier in green chemical synthesis.[37–40] Unlike conventional thermal catalytic processes, which typically require harsh reaction conditions[41] and high energy inputs,[19] the electrocatalytic pathway leverages renewable electricity to directly couple reactive nitrogen species with diverse carbon-based substrates, including CO_2 and its electroreduction-derived intermediates, aldehydes and ketones, and biomass-derived active intermediates, offering a sustainable alternative to traditional thermochemical approaches. The resulting products encompass a broad spectrum of important chemicals, such as oximes,[42–44] amino acids,[45–47] amines,[48–50] amides,[51–53] urea[54–57] and heterocyclic compounds (Fig. 1), which are essential intermediates in agriculture, pharmaceuticals, materials, and environmental remediation.[58]

Among these versatile transformations, several representative NO_x-involved C–N coupling reactions have been intensively studied. For instance, reductive amination reactions involving nitrate or nitrite and carbonyl substrates afford high-value oximes, amines, amino acids, etc.[59–61] Similarly, the electrochemical synthesis of urea from CO_2 and NO_x provides an attractive route to sustainably produce urea fertilizers.[62] These

C–N coupling reactions expand the scope of green electrosynthesis to complex organic molecules traditionally synthesized using multi-step pathways.[63–67]

In recent years, substantial progress has been made in identifying suitable substrates and demonstrating the feasibility of electrochemical C–N coupling reactions.[68] Meanwhile, aided by advances in theoretical modelling, computational simulations and in situ/operando characterization techniques, electrochemical catalysis has enabled researchers to gain deeper insights into the composition and configuration of key intermediates, evaluating their binding affinities and regulating the catalytic activity and product selectivity of these systems.[69–76] However, due to the multi-step electron/proton transfer processes, as well as various reactive chemical bonds, active intermediates, and competing reaction pathways, these reactions become more complex.[32,71,77] A central challenge lies in controlling the reaction selectivity and preventing side reactions such as hydrogen evolution reaction (HER), over-hydrogenation, and undesired side-reaction.[78–81] Consequently, minor fluctuations in the electrode surface properties,[82–85] active intermediate binding energies,[86] or local reaction microenvironments[87–89] can drastically alter the product distribution and overall reaction efficiency.[8,71] Furthermore, achieving simultaneous optimal adsorption and activation of disparate reactants (such as NO_x and carbon sources) poses significant challenges.[90–92] Different reactants typically require different binding sites and distinct electronic environments, making it difficult to align the reaction pathways on single-site or homogeneous catalyst surfaces.[93] At the same time, conventional catalyst designs rely on static structures, which fail to accommodate the dynamic structural and electronic changes occurring during electrocatalysis.[94] If these mechanistic and catalytic challenges are not effectively solved, they would severely hinder the transition of electrocatalytic C–N coupling processes from laboratory-scale demonstrations to practical, large-scale applications.

Thus, to overcome these intrinsic mechanistic limitations and to further enhance the performance of electrocatalytic NO_x-involved C–N coupling reactions, researchers have proposed five representative catalyst engineering strategies (Fig. 2), including defect engineering, coordination environment design, interface engineering, dual-site synergy and emerging architectures. By resolving challenges such as the instability of the reactive intermediates, the occurrence of competing side reactions, and the mismatch in substrate adsorption requirements, these approaches collectively enhance the effectiveness of C–N bond construction under electrochemical conditions.

In this paper, we provide a comprehensive overview of electrocatalytic C–N coupling reactions involving NO_x species from the perspective of catalyst design strategies. We systematically categorize the recent advances into five major approaches including defect engineering, coordination environment design, interface engineering, dual-site synergy, and emerging architectures. These strategies can regulate the structural and

Buxing Han has been a professor at ICCAS since 1993. He is Academician of Chinese Academy of Sciences and Fellow of the Royal Society of Chemistry; a titular member of the Organic and Biomolecular Chemistry Division, IUPAC; and was the Chairman of the IUPAC Subcommittee on Green Chemistry from 2008 to 2012. He works in the interdisciplinary area of Physical Chemistry and Green Chemistry. His research interests include the properties of green solvent systems and applications of green solvents in chemical reactions and material science.

Buxing Han

This journal is © the Partner Organisations 2025

Inorg. Chem. Front., 2025, **12**, 6926–6945 | **6927**
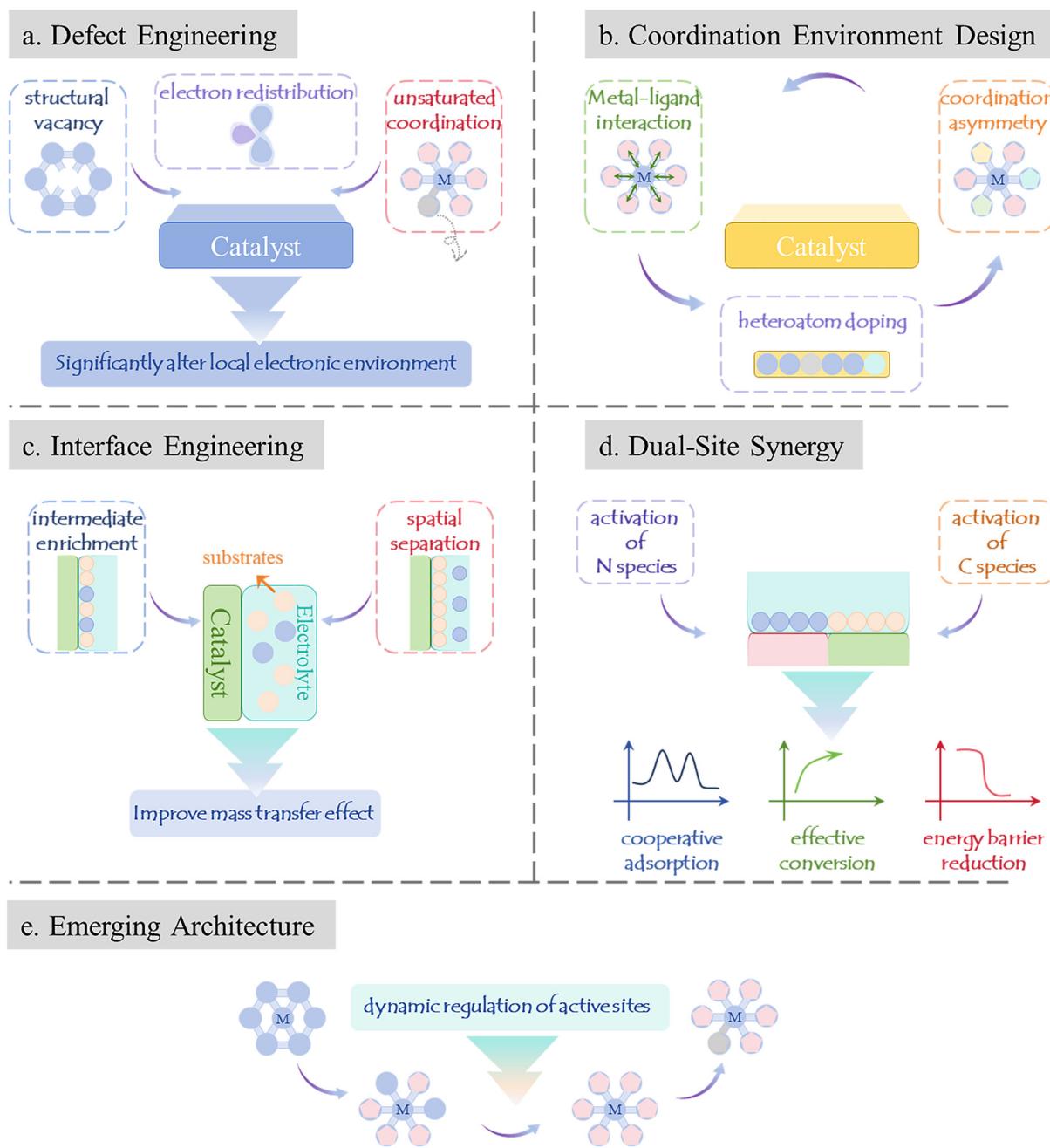
Fig. 2 Schematic of five catalyst design strategies for electrocatalytic C−N coupling. (a) Defect engineering: modulating local electronic environments *via* structural vacancies, unsaturated coordination, and electron redistribution. (b) Coordination environment design: optimizing active sites through metal−ligand interactions and asymmetric coordination. (c) Interface engineering: enhancing mass transfer by spatial separation and substrate-enriched microenvironments. (d) Dual-site synergy: cooperatively activating N/C species to reduce C−N coupling barriers. (e) Emerging architectures: dynamically regulating active sites for adaptive reaction pathways. Collectively, these strategies address bottlenecks in electron transfer, mass transport, and dynamic instability during NO_x conversion.

electronic characteristics, helping to resolve key issues in intermediate stabilization, substrate adsorption and reaction selectivity. In addition, the last section outlines the challenges and development prospects for NO_x-involved C−N coupling. We believe that this review can inspire new exploration and principles for catalyst design for electrocatalytic C−N coupling reactions.

2 Catalyst design strategies for NO_x-involved C−N coupling

Defect engineering represents a fundamental approach wherein the deliberate introduction of structural vacancies, unsaturated coordination sites, or electronic redistributions significantly alters the

6928 | *Inorg. Chem. Front.*, 2025, **12**, 6926−6945

This journal is © the Partner Organisations 2025

local electronic environments[60] of catalysts (Fig. 2a). These engineered defects can act as highly active adsorption and activation centers, precisely tune the binding energy of the key intermediates and lower the activation barriers for critical C–N coupling steps. This precise electronic control at defect sites provides an effective solution for stabilizing the elusive intermediates, thereby significantly improving the overall catalytic selectivity and efficiency.

The second category is coordination environment design, emphasizing the adjustment of the local atomic arrangement around the active metal center (Fig. 2b). Through rational tuning of the metal–ligand interactions, heteroatom incorporation, and coordination asymmetry, catalysts are able to influence the intermediate adsorption behavior and energy barriers, thereby promoting more selective and efficient C–N bond formation.[95]

Interface engineering, as the third major strategy, focuses on regulating the physicochemical properties at the boundary between different phases to construct favorable local microenvironments at the interface between the electrode and electrolyte (Fig. 2c). By tuning the interfacial characteristics such as surface polarity, wettability, and spatial distribution of reactants, this approach can facilitate selective intermediate enrichment, improve the mass transport, and spatially separate the reaction steps.[44] As a result, interface engineering electrocatalytic systems often demonstrate improved reaction selectivity, enhanced stability, and better compatibility with complex multi-step C–N coupling processes.

Dual-site synergy enhances the performance of NO_x-involved C–N coupling reactions by integrating two types of catalytic active centers with complementary effects in a single system (Fig. 2d). Typically, one site promotes the activation of nitrogen-containing species, while the other is responsible for the activation of carbon-containing species.[96] The spatial proximity and electronic complementarity between the two sites promote synergistic adsorption, efficient intermediate transfer, and selective C–N bond formation.[97] This cooperative mechanism improves overall reaction coordination, lowers the energy barrier, and helps to suppress undesirable side reactions, thereby contributing to improved activity and selectivity in complex multistep transformations.

Emerging architectures introduce a new design perspective, emphasizing the adaptability and responsiveness (Fig. 2e). Rather than relying solely on rigid structural parameters, this strategy focuses on dynamic regulation of the active sites and structural evolution during the reaction process,[98] offering opportunities to balance the activity and selectivity across complex pathways and opening up new directions for intelligent, programmable and multi-step coupling catalytic platforms.

3 Representative cases in the literature

3.1 Defect engineering

Defect engineering offers a powerful strategy to tailor the local electronic environment of electrocatalysts by introducing vacancies, unsaturated coordination sites, and charge redistributions. These defect-induced modulations profoundly influence the adsorption configurations, intermediate stabilization, and activation barriers associated with NO_x- and carbon-based species. Particularly, defect sites can serve either as highly active centers for C–N bond formation or as electronic reservoirs that stabilize the key intermediates, thereby suppressing competing reactions and steering the reaction toward selective coupling pathways. By precisely tuning the type, density, and spatial distribution of defects, recent studies have demonstrated enhanced coupling efficiency, optimized reaction energetics, and improved selectivity across various electrocatalytic systems for the synthesis of value-added nitrogenous products.

Xian and co-workers developed a catalyst based on atomically dispersed Fe–N_4 sites anchored in a nitrogen-doped carbon matrix (AD-Fe/NC), aiming to achieve precise control over amino acid electrosynthesis via defect-engineered local electronic redistribution.[60] In the AD-Fe/NC catalyst, the Fe–N_4 centers act as electron-deficient sites, where potential-driven orbital rearrangement enhances NO adsorption and facilitates the formation of key intermediates (Fig. 3a), thereby promoting the C–N coupling step. Under an applied potential of −0.6 V vs. reversible hydrogen electrode (RHE), the catalyst achieved a valine yield of 32.1 μmol mg_{cat}^{-1} with a selectivity of 11.3%, demonstrating excellent capability for the high-value conversion of nitrogen oxides.

Fan et al. developed a Pd/Cu-V_{Cu} electrocatalyst based on defect engineering by introducing Cu vacancies to modulate the local electronic structure of Cu nanosheets,[99] which exhibited remarkable activity for the electrochemical synthesis of N,N-dimethylformamide (DMF) from CO_2 and dimethylamine (DMA). The introduction of Cu vacancies (Cu-V_{Cu}) into the Cu nanosheets modulated their local electronic structure, significantly enhancing CO_2 adsorption and facilitating spontaneous coupling with DMA to form C–N bonds (Fig. 3b). Concurrently, Pd nanoparticles accelerated the electrochemical reduction of the key intermediate *$OCN(CH_3)_2OH$ to $OCHN(CH_3)_2OH$, thereby markedly improving the overall efficiency of DMF formation (Fig. 3c). Under an applied potential of −0.6 V vs. RHE, the catalyst achieved a high DMF yield of 385 mmol h^{-1} g_{cat}^{-1} and a faradaic efficiency (FE) of 37.5%. Density functional theory (DFT) calculations further revealed that the introduction of copper vacancies led to electronic redistribution, which reduced the energy barriers for C–N bond formation, facilitated proton-coupled electron transfer, and enhanced the kinetics of intermediate hydrogenation.

Pan and co-authors developed vacancy-rich electrochemically oxidation-derived copper (e-OD-Cu) for the efficient synthesis of hexamethylenetetramine (HMTA) via electrochemical C–N coupling between nitrate and formaldehyde.[100] The presence of Cu vacancies significantly enhanced the adsorption of NO_3^- and HCHO, thereby facilitating the initial steps of the reaction cascade (Fig. 3d). The nitrate was first reduced to *NH_3 through a multi-electron pathway, which then reacted with *HCHO to form imine-type intermediates (Fig. 3e).

This journal is © the Partner Organisations 2025

Inorg. Chem. Front., 2025, 12, 6926–6945 | 6929
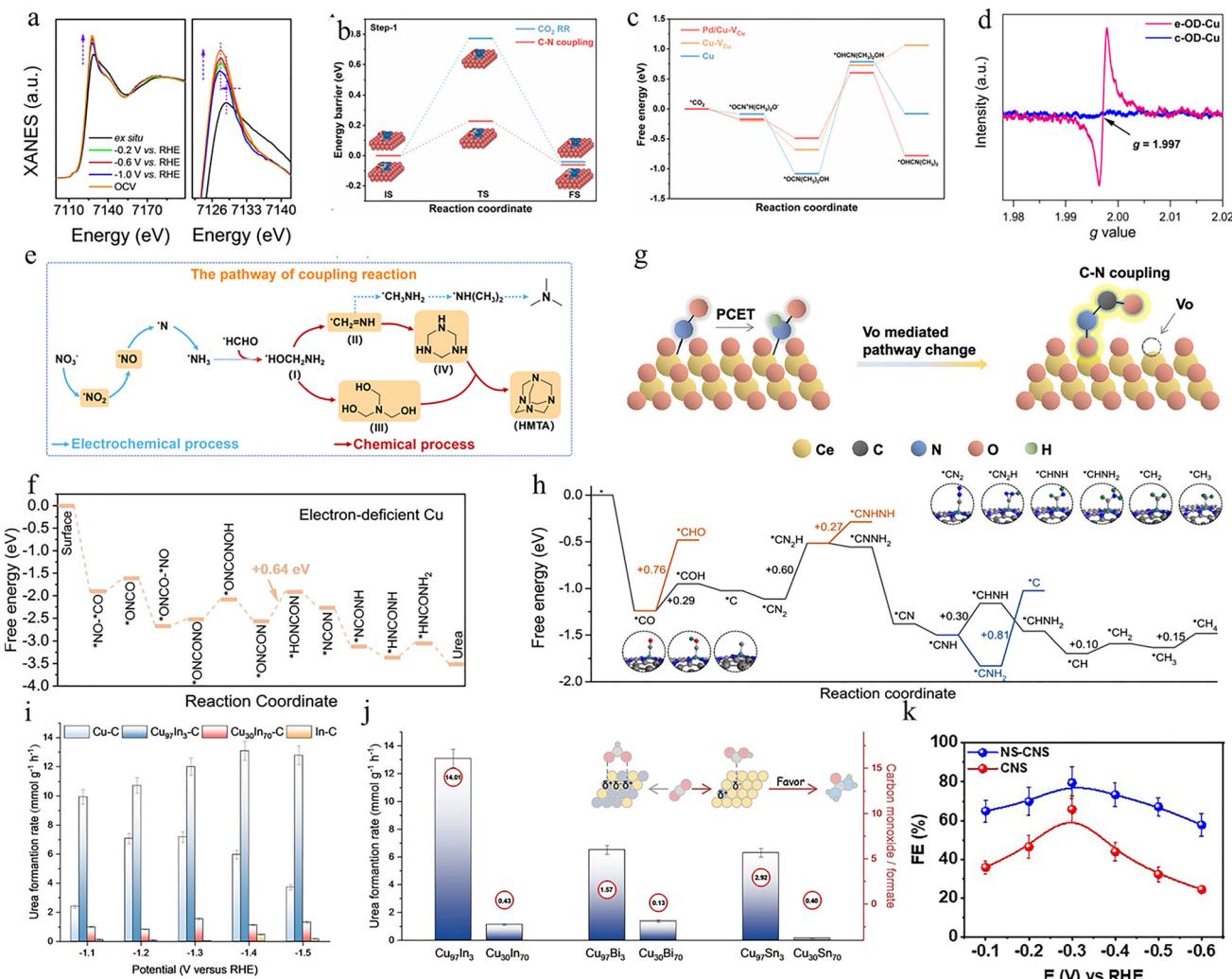
Fig. 3 (a) *In situ* Fe K-edge XANES spectra of AD-Fe/NC under applied potentials from OCV to −1.0 V *vs.* RHE. The white-line intensity attenuation at −1.0 V indicates Fe valence reduction during reductive amination.[60] Reproduced with permission from ref. 60, Copyright © 2023, Wiley-VCH GmbH. (b) Gibbs free energy change (Δ*G*) for CO₂ reduction to *OCHO intermediate and subsequent C–N coupling on Pd/Cu-V$_{Cu}$.[99] (c) Comparative Gibbs free energy profiles for DMF synthesis on pure Cu, Cu-V$_{Cu}$, and Pd/Cu-V$_{Cu}$ surfaces.[99] Reproduced with permission from ref. 99, Copyright © 2024, Elsevier Inc. (d) Electron paramagnetic resonance (EPR) spectra of c-OD-Cu and e-OD-Cu. The distinct signal at *g* = 1.997 for e-OD-Cu indicates the presence of unpaired electrons trapped at copper vacancy sites, while no significant signal is observed for c-OD-Cu.[100] (e) Schematic of the tandem electrochemical-chemical pathway for electrocatalytic HMTA synthesis from nitrate and formaldehyde.[100] Reproduced with permission from ref. 100, Copyright © 2024, the American Chemical Society. (f) Free energy profiles for urea synthesis pathways on electron-deficient Cu (Cu/PI-500).[101] Reproduced with permission from ref. 101, Copyright © 2024, Wiley-VCH GmbH. (g) Schematic of oxygen vacancy (V$_O$)-mediated reaction pathway switching on CeO₂.[102] Copyright © 2022, the American Chemical Society. (h) Free energy profile for nitrogen reduction reaction (NRR) elementary steps on *C-modified ReMn-NC.[101] Reproduced with permission from ref. 101, Copyright © 2024, Elsevier Inc. (i) Urea yield rates under applied potential for Cu–C, Cu₉₇In₃₋C, Cu₃₀In₇₀₋C, and In–C electrocatalysts.[62] (j) Urea yield rates and CO/HCOO⁻ molar ratios across bimetallic Cu–In, Cu–Bi, and Cu–Sn electrocatalysts.[62] Reproduced with permission from ref. 62, Copyright © 2023, Wiley-VCH GmbH. (k) FE of the production for NS-CNS (blue), CNS (red).[104] Reproduced with permission from ref. 104, Copyright © 2023, Elsevier.

Notably, the Cu vacancies played a critical role in suppressing the over-hydrogenation of the *CH₂=NH intermediate, effectively steering the reaction away from undesired byproducts and enabling the progressive formation of multi-substituted amine intermediates. This promoted tandem condensation and ring-closing reactions, which ultimately yielded HMTA with an FE of 74.9% and yield of 76.8% at −0.30 V *vs.* RHE.

Wang *et al.* constructed electron-deficient Cu sites *via* strong metal-polyimide (PI) semiconductor interactions (named Cu/PI-*X* catalyst, where *X* represents the thermal treatment temperature on PI), enabling efficient urea synthesis through the electrocatalytic coupling of nitrate and carbon dioxide.[101] The electron-deficient Cu/PI-500 significantly enhanced the co-adsorption of *NO and *CO intermediates

and stabilized the key intermediates (*e.g.* *ONCONO), thus reducing the reaction energy barriers for sequential C–N bond formation (Fig. 3f). Cu/PI-500 delivered a high urea yield rate of 255.0 mmol h^{-1} g^{-1} and FE of 14.3% at −1.4 V *vs.* RHE, with outstanding electrochemical durability.

Wei *et al.* developed a CeO$_2$-supported Cu catalyst enriched with oxygen vacancies (V$_O$-CeO$_2$-750) to enable the electrocatalytic coupling of nitrate and carbon dioxide for urea synthesis.[102] The introduction of Vo sites significantly reshaped the local electronic structure of CeO$_2$, enabling strong stabilization of the *NO intermediate and favoring its coupling with *CO to form the key *OCNO species (Fig. 3g). By anchoring the *NO intermediates *via* V$_O$, the catalyst raises the *NO hydrogenation barriers by 0.12 eV, while reducing the *NO–*CO coupling barriers to 0.27 eV (48% decrease). As a result, the catalyst achieved a high urea yield of 8.81 mmol h^{-1} g$_{cat}^{-1}$ and FE of 12.2% at −0.7 V *vs.* RHE.

Zhang and co-workers proposed a "Janus C–N coupling" strategy for the selective synthesis of ammonia and urea under ambient conditions, using nitrogen, carbon dioxide, water and electricity as feedstocks.[103] Specifically, an Re–Mn dual-atomic electrocatalyst (ReMn-NC) with strong CO adsorption was constructed, facilitating the formation of *C intermediates, which acted as electron reservoirs. These electron-rich *C species promoted end-on adsorption and subsequent C–N coupling with nitrogen (N$_2$ + *C → *CN$_2$, Fig. 3h). Subsequent hydrogenation of *CN$_2$, accompanied by C–N dissociation, selectively produced ammonia at a remarkable yield of 48.9 mg g^{-1} h^{-1} and a nitrogen selectivity of 98.4%. Conversely, a Zn–Mn dual-atomic electrocatalyst (ZnMn-NC) exhibiting low Co binding strength facilitated the release and migration of CO, enabling its coupling with adsorbed nitrogen (CO + *N≡N* → *NCON*). Subsequent hydrogenation of the nitrogen atoms efficiently yielded urea, achieving an average yield rate of 36.7 mg g^{-1} h^{-1} and nitrogen selectivity of 89.1%. Notably, modulating the local electronic states of catalysts significantly influences the electronic density distribution at their active sites, directly affecting the stability and activity of adsorbed species, and thereby facilitating the synergistic development of nitrogen reduction and C–N coupling reactions.

Beyond the aforementioned strategies, modulation of the local electronic states (such as redistribution of localized charge density) constitutes defect engineering at the electronic-structure level. By profoundly altering the adsorption configurations of the intermediates and steering the catalytic reaction pathways, this strategy enables the efficient electrocatalytic synthesis of target chemicals. Liu *et al.* demonstrated efficient electrocatalytic urea synthesis under ambient conditions by tuning the local electronic state of bimetallic electrocatalysts using CO$_2$ and NO$_3^-$ reactants.[62] They found that the localized surface charge of the catalysts significantly influenced the adsorption configurations of the CO$_2$ intermediates and subsequent reaction pathways. Specifically, the negatively charged Cu$_{97}$In$_{3-C}$ surface preferentially induced the formation of C-bound *COOH intermediates, greatly enhancing the subsequent C–N coupling reactions and resulting in an impressive

urea yield rate of 13.1 mmol g^{-1} h^{-1}, which is about 13 times higher than that of the positively charged Cu$_{30}$In$_{70-C}$ surface (dominated by O-bound *OCHO intermediates, as shown in Fig. 3i). Mechanistic studies revealed that the negatively charged surfaces facilitated the stable adsorption of reactive intermediates through the formation of C-bound configurations, significantly improving the urea synthesis performance. Conversely, positively charged surfaces promoted the formation of O-bound intermediates, creating a dead-end for subsequent C–N coupling, and thus substantially reducing the urea yield (Fig. 3j). This precise regulation of the adsorption configurations and reaction pathways *via* localized electronic state tuning exemplifies the critical role of defect engineering in electrocatalytic urea synthesis.

Jia *et al.* utilized a defect engineering strategy by developing nitrogen and sulfur co-doped lignin-derived carbon nanosheets (NS-CNS) for the efficient electrocatalytic reductive amination of pyruvate to alanine.[104] Co-doping with nitrogen and sulfur effectively modulated the localized electronic states on the catalyst surface, significantly enhancing the local electron density distribution at the carbon active sites, thereby improving the adsorption affinity toward the critical imine intermediates and lowering the reaction energy barrier. Specifically, the localized electron-rich sites facilitated the rapid reduction of the imine intermediates to alanine, while simultaneously suppressing competing side reactions, such as hydrogen evolution. Under the optimized reaction conditions (−0.3 V *vs.* RHE), the NS-CNS catalyst exhibited an impressive FE of 79.5% with the alanine yield reaching up to 199 mmol h^{-1} cm^{-2} and selectivity exceeding 99.9% (Fig. 3k). Additionally, the catalyst demonstrated remarkable stability for long-term electrocatalytic processes and showed excellent potential for practical applications, as evidenced by successfully converting real-world polylactic acid waste into value-added alanine with selectivity greater than 75%.

3.2 Coordination environment design

The coordination environment surrounding the active metal centers plays a fundamental role in determining the activity, selectivity, and stability of electrocatalysts involved in NO$_x$-related C–N coupling reactions. Rather than merely relying on the elemental composition of catalysts, recent advances have demonstrated that adjusting the coordination configuration, such as through heteroatom incorporation, low-coordination site construction, and asymmetry induction, can effectively tune their local electronic structure and reactivity. These coordination design strategies regulate the adsorption behavior of the NO$_x$ species and stabilize the key nitrogen-containing intermediates such as *NH$_2$OH and oximes, while suppressing side processes such as HER and over-reduction. By leveraging diverse coordination motifs across nanostructured, alloyed, and molecular catalyst systems, researchers have created favorable reaction microenvironments that promote efficient multi-electron transfer and selective C–N bond formation. The following section highlights several representative studies where coordination environment engineering serves as

This journal is © the Partner Organisations 2025

*Inorg. Chem. Front.*, 2025, **12**, 6926–6945 | **6931**

a powerful means to guide catalytic transformations at the atomic level.

Kang and co-workers proposed an interfacial coordination strategy by anchoring a Zn-based metal–organic framework (ZIF-7) onto carboxyl-functionalized graphite felt (CGF), which was named ZIF-7/CGF,[43] where Zn–O bridges were formed between the MOF and the substrate. This modification induced the transformation of the Zn coordination environment from a symmetric Zn–N_4 tetrahedral configuration to an asymmetric Zn-N_3O structure. *In situ* XAFS analysis revealed that the Zn sites underwent *in situ* reconstruction, characterized by a reduction in the Zn coordination number from 4.0 to 3.3 and an increase in the average Zn–ligand bond length (Fig. 4a). Compared with the conventional Zn–N_4 sites, the Zn-N_3O configuration not only enhanced the NO adsorption capacity but also facilitated the formation and desorption of the NH_2OH intermediate, thereby promoting the key C–N coupling pathway.

Wu *et al.* reported a sulfur-modified copper electrocatalyst (Cu–S) that leverages interface engineering to precisely regulate the surface reaction environment for electrochemical C–N coupling between nitrite and cyclohexanone, attaining a remarkable product selectivity of 99% and yield of 92% at −0.9 V *vs.* Ag/AgCl.[42] The superior performance originated from the tailored Cu–S coordination structure, which modulated the electronic configuration of the Cu active sites. The appearance of the Cu–S configuration weakened the over-reduction of NH_2OH^*. *In situ* ATR-SEIRAS spectroscopy (Fig. 4b) further demonstrated that NH_2OH^* remains stably adsorbed on the surface and undergoes direct coupling with cyclohexanone, enabling selective oxime formation.

Sheng *et al.* constructed a porous high-entropy alloy metallene catalyst (HEA-PdCuAgBiInene), which demonstrates an effective coordination environment modulation strategy for promoting C–N coupling electrosynthesis.[95] The incorporation of p-block metals (Bi, In) into the PdCuAg matrix induces
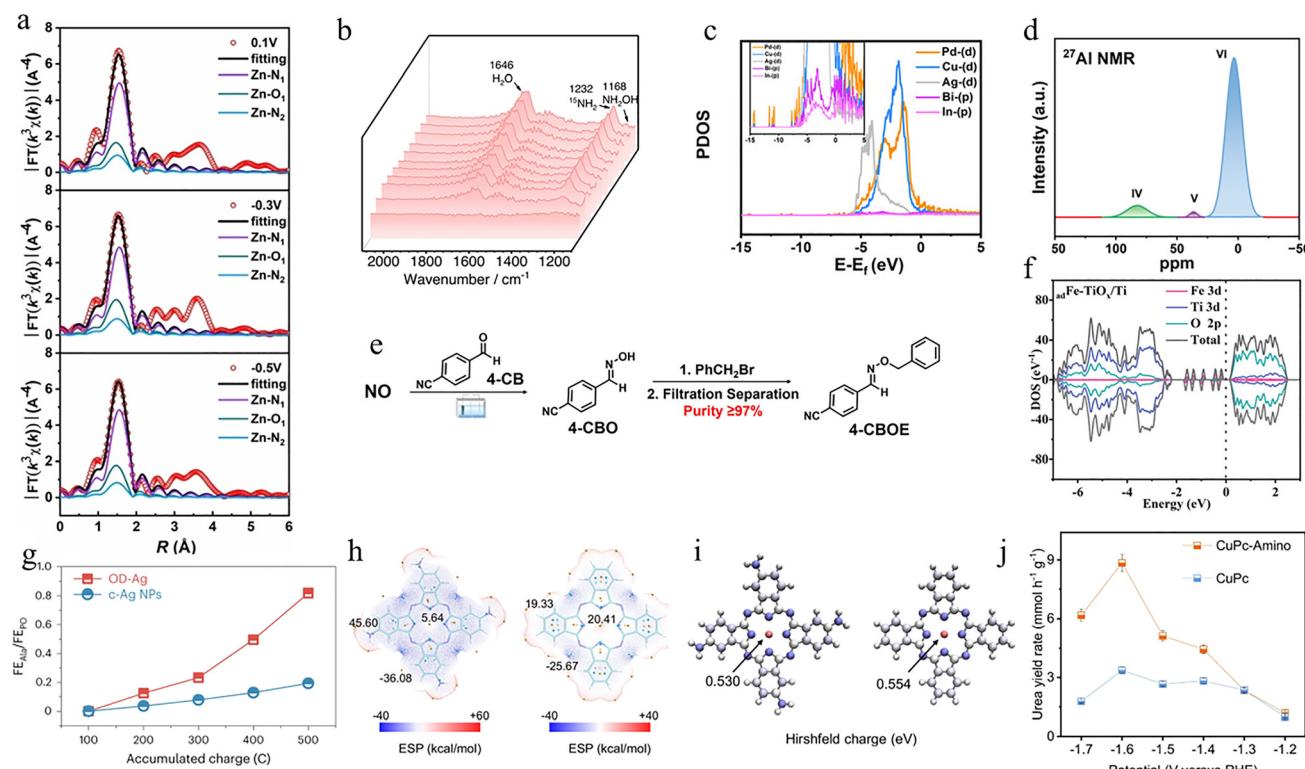
Fig. 4 (a) Fitting curves recorded at the Zn K-edge under working conditions.[43] Reproduced with permission from, ref. 43 Copyright © 2025, Springer Nature. (b) Time-dependent *in situ* ATR-SEIRAS was carried out using isotopically labeled $^{15}NO_2^-$ as the N source and H_2O as the H donor.[42] Reproduced with permission from ref. 42, Copyright © 2023, Springer Nature. (c) PDOS of HEA-PdCuAgBiIn with the p–d orbital hybridization given in the inset.[95] Reproduced with permission from ref. 95, Copyright © 2024, Wiley-VCH GmbH. (d) Distribution of aluminum coordination states in Al-NFM.[105] Reproduced with permission from ref. 105, Copyright © 2023, Wiley-VCH GmbH. (e) Schematic of the synthesis of 4-CBOE from NO and 4-CB.[106] Reproduced with permission from ref. 106, Copyright © 2024, Wiley-VCH GmbH. (f) Projected density of states (PDOS) and total density of states (TDOS) plots of $_{ad}Fe-TiO_x/Ti$.[107] Reproduced with permission from ref. 107, Copyright © 2024, Wiley-VCH GmbH. (g) Comparison of FE_{Ala}/FE_{PO} ratios over OD-Ag and commercial Ag nanoparticles (c-Ag NPs) during NO and pyruvic acid electrolysis. The gradually increasing FE_{Ala}/FE_{PO} ratio over OD-Ag with accumulated charge highlights its superior activity in oxime (PO) reduction, while c-Ag NPs show limited conversion efficiency.[47] Reproduced with permission from ref. 47, Copyright © 2023, Springer Nature. (h) Electrostatic potential (ESP) analysis for CuPc-Amino and CuPc.[108] (i) Electronic charge redistribution patterns examined through Hirshfeld charges analysis for CuPc-Amino relative to its unsubstituted CuPc.[108] (j) Urea synthesis partial current densities for both CuPc-Amino and CuPc catalysts measured across a range of applied potentials.[108] Reproduced with permission from ref. 108, Copyright © 2024, Springer Nature.

6932 | *Inorg. Chem. Front.*, 2025, **12**, 6926–6945

This journal is © the Partner Organisations 2025

unconventional p–d orbital hybridization, which leads to local electron enrichment and d-state localization at the Pd active sites (Fig. 4c). This tailored coordination environment fine-tunes the adsorption energies of hydrogen and NO_2^--derived intermediates, suppresses the over-hydrogenation of NH_2OH^*, and facilitates its selective condensation with surface-enriched cyclohexanone ($C_6H_{10}O^*$). The HEA catalyst achieved an FE of 47.6% and nearly 100% yield under mild electrochemical conditions (−0.9 V vs. Ag/AgCl), offering a compelling example of active-site engineering via orbital-level coordination control.

Xiang et al. developed an aluminum-containing nanofiber membrane catalyst (Al-NFM) derived from NH_2-MIL-53(Al)[105] for the electrosynthesis of pyridine oximes via the in situ reduction of NO_2^- to NH_2OH^*. The catalyst possesses a highly disordered carbon structure with abundant defect sites and a mixture of six-, five-, and four-coordinated Al centers, of which approximately 20% are coordinatively unsaturated. These Al–N motifs modulate the local electronic environment, promote NO_2^- activation, and stabilize the NH_2OH^* intermediate, as supported by the charge distribution analysis and energy profile calculations (Fig. 4d). The absence of Al or nitrogen doping led to significantly lower NH_2OH yields and reduced product selectivity, underscoring the essential role of coordination tuning. Operating at −0.9 V vs. Ag/AgCl under ambient conditions, Al-NFM achieved an FE of 42.1% and 92.1% selectivity.

Wang and co-authors reported a one-pot electrosynthesis strategy for the production of oxime ether by NO_x reduction and aldehyde activation using ultrafine MgO nanoparticles embedded in nitrogen-doped carbon nanofiber membranes (MgO-SCM).[106] The electrosynthesis process targets the efficient one-pot conversion of NO_x and 4-cyanobenzaldehyde (4-CB) to 4-cyanobenzaldoxime (4-CBO), and subsequently to its oxime ether (4-CBOE) under ambient conditions, as shown in Fig. 4e. In this system, the catalyst is derived from Mg-MOFs, and the Mg–O coordination structure was largely preserved during thermal decomposition, forming well-dispersed MgO active sites. This preserved coordination environment generated abundant acid–base pairs on the surface of MgO, which played a key role in steering the NO_x reduction pathway, while the highly dispersed MgO nanoparticles embedded in the N-doped carbon matrix facilitate preferential NO adsorption, limiting the HER activity. This fine control over surface coordination enables the production of 4-CBOE with 93% selectivity and 65.1% FE at 12 mA.

Zhu and co-authors developed an atomically dispersed iron-supported defect TiO_2 electrocatalyst ($_{ad}$Fe-TiO_x/Ti) that synergistically integrates oxygen vacancies (OVs) and isolated Fe sites to facilitate C–N coupling reactions for α-amino acid synthesis.[107] The defect-rich TiO_2 matrix was designed to introduce a large number of OVs, while Fe atoms were anchored at these vacant positions to form a uniformly dispersed Fe–O coordination structure. The formation of Fe–O_3 complexes enhances the electronic interaction between Fe and the defective oxide support (Fig. 4f). OVs promoted the adsorption of nitric acid (NO_3^-), glyoxylic acid (GA) and glyoxylic oxime (GO),

while $_{ad}$Fe significantly reduced the energy barrier for the conversion of NO_3^- to NH_2OH and GO to glycine. A glycine yield of 80.2% was achieved using the $_{ad}$Fe-TiO_x/Ti catalyst with GA conversion close to 100%.

Li et al. developed a coordination-modulated Ag-based catalyst to realize the electrosynthesis of alanine from NO and pyruvic acid.[47] The oxide-derived Ag (OD-Ag) exhibits a reduced average coordination number (CN ≈ 7.2), which leads to under-coordinated Ag sites with altered surface electronic structures. These modified coordination environments enable the stronger adsorption of the oxime intermediates and lower the energy barriers for the key transformation step, including N–O bond cleavage and C=N hydrogenation. Compared to commercial Ag nanoparticles, OD-Ag significantly boosts the pyruvate oxime (PO)-to-alanine conversion rate, while suppressing side HER processes (Fig. 4g). The coordination-induced activity enhancement is further supported by DFT calculations, showing favorable charge redistribution and reduced activation energy on low-coordinated sites.

The in research by Li and co-workers, they utilized the ligand engineering strategy exemplified by CuPc-amino, demonstrating how coordination environment modulation enhances electrocatalytic urea synthesis.[108] Amino substitution strengthens the intramolecular Cu–N coordination (coordination number increased from 3.9 to 4.2), while simultaneously optimizing the electronic structure through the reduction of the Cu site electrostatic potential from 20.41 to 5.64 kcal mol^{-1} (Fig. 4h). This coordination environment modification effectively suppresses electrochemical demetallation and promotes the adsorption of the key *CO and *NO intermediates for C–N coupling (Fig. 4i). The engineered CuPc-amino catalyst achieved a remarkable urea yield rate of 103.1 ± 5.3 mmol h^{-1} g^{-1} at −1.6 V vs. RHE (Fig. 4j), representing a 2.6-fold improvement over unmodified CuPc, while maintaining near-zero activity decay over 10 cycles compared to the 67.4% decay observed for CuPc.

3.3 Interface engineering

Interface engineering involves the rational design and control of regions where two or more phases intersect, including solid–liquid interfaces and multiphase interface such as solid–liquid–gas and oil–water–gas interfaces.[83,109] These interface regions often exhibit unique electron transfer, reaction environment, reaction environments, and mass transfer properties. In the C–N coupling reaction, multiphase interfaces can enhance the reactant enrichment, stabilize the key intermediates, and provide spatial separation of the reaction steps. Therefore, interface engineering serves as a powerful strategy to promote multi-step catalytic pathway/multi-electron transfer pathways and improve the efficiency of C–N bond formation.

A representative example of multiphase interface design is the Pickering emulsion droplet-integrated electrode developed by Zhang et al., which enables the continuous-flow electrosynthesis of cyclohexanone oxime from NO and cyclohexanone.[44] In this system, the catalyst Ag-50 is composed of silver nanoparticles modified by polypyrrole, which has both the

This journal is © the Partner Organisations 2025

Inorg. Chem. Front., 2025, **12**, 6926–6945 | **6933**
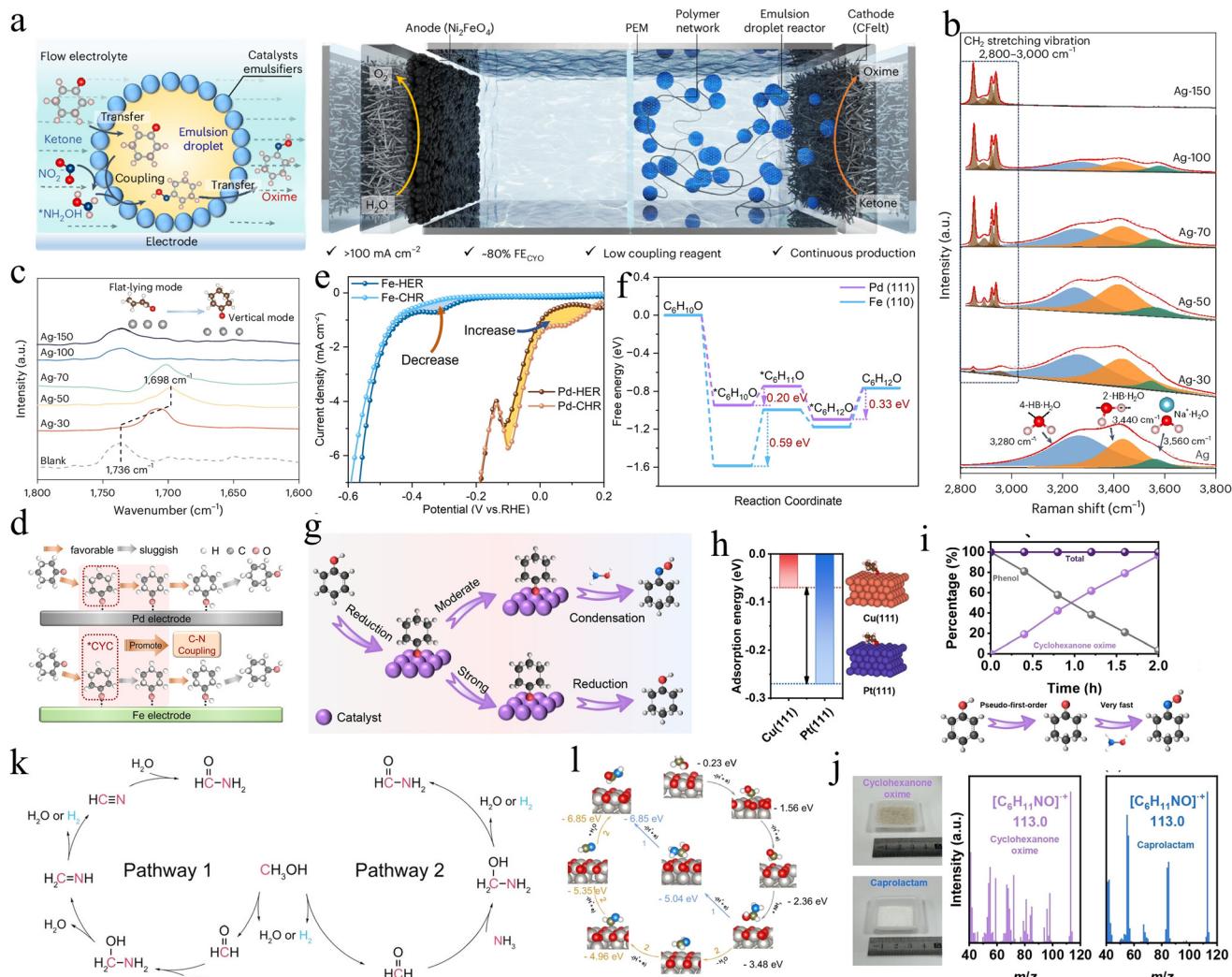
Fig. 5 (a) Illustration of a continuous-flow system for cyclohexanone oxime synthesis enabled by electrode-integrated Pickering emulsions. The structured oil–water interface formed by the emulsion droplets offers a confined reaction environment that facilitates efficient oxime formation at high current densities.[44] (b and c) Raman and *in situ* FTIR were employed to probe the oil–water interfacial region in the Pickering emulsion system, revealing the hydrogen-bonding network and the adsorption configuration of cyclohexanone.[44] Reproduced with permission from ref. 44, Copyright © 2025, Springer Nature. (d) Illustration mechanisms of the cyclohexanone hydrogenation reaction (CHR) pathways on Pd and Fe surfaces, highlighting differences in intermediate adsorption and hydrogenation tendencies at the interface.[78] (e) Line sweep voltammetry (LSV) curves comparing the hydrogen evolution (HER) and CHR performance on Pd and Fe electrodes.[78] (f) Calculated free energy diagrams of the CHR on Pd(111) and Fe(111) surfaces.[76] Reproduced with permission from ref. 78, Copyright © 2023, Wiley-VCH GmbH. (g) Schematic of the adsorption of cyclohexanone on different catalysts' surfaces.[59] (h) Free energy of cyclohexanone intermediates on the Cu (111) and Pt (111) models.[61] (i) Time-dependent kinetic profile for cyclohexanone oxime formation on Cu at −0.9 V (top), and schematic of the phenol-to-oxime reaction pathway (bottom).[61] Reproduced with permission from ref. 61, Copyright © 2024, Wiley-VCH GmbH. (j) GC results and photos of reaction products.[61] Reproduced with permission from ref. 61, Copyright © 2024, Wiley-VCH GmbH. (k) Possible reaction pathway for the electrooxidation of CH_3OH and NH_3 coupling to form $HCONH_2$ on BDD.[110] Reproduced with permission from ref. 110, Copyright © 2022, Wiley-VCH GmbH. (l) Theoretical model of formamide formation pathways on the surface of α-PtO_2.[111] Reproduced with permission from ref. 111, Copyright © 2022, Springer Nature.

functions of a catalyst and a Pickering emulsifier. It assembles at the oil–water interface and stabilizes the emulsion micro-reactor on the electrode surface (Fig. 5a). The interface environment promotes the selective enrichment and alignment of the oil phase cyclohexanone and water phase NH_2OH. *In situ* ATR-FTIR (Fig. 5b) and Raman spectroscopy (Fig. 5c) revealed an asymmetric hydrogen-bonding network formed by interfacial water, aligning the cyclohexanone molecules

vertically on the surface and promoting nucleophilic attack by NH_2OH. This unique interfacial configuration enhances the nucleophilic attack of NH_2OH and suppresses its over-reduction to NH_3, thereby improving the C–N coupling efficiency. Under industrial-level current densities (100 mA cm^{-2}), the system achieved an FE of 83.8% and yield of 0.78 mmol h^{-1} cm^{-2}. Further immobilization of the emulsion droplets using polypyrrole cross-linking allowed the gram-scale

6934 | *Inorg. Chem. Front.*, 2025, **12**, 6926–6945

This journal is © the Partner Organisations 2025

synthesis of oxime in continuous flow, highlighting the power of interfacial engineering in biphasic electrocatalysis.

Wu *et al.* designed a biphasic electrochemical system for the synthesis of cyclohexanone oxime from NO_x and cyclohexanone (CYC), achieving a nearly 100% yield on Fe-based electrocatalysts under flow conditions.[78] In this system, NO_x and CYC from two immiscible phases accumulate simultaneously on the Fe surface, forming $*NH_2OH$ and $*CYC$ as adsorbed intermediates (Fig. 5d). Fe exhibits stronger adsorption for CYC but weaker hydrogenation ability compared to Pd (Fig. 5e), thus preventing over-reduction and ensuring $*CYC$ availability for C–N coupling. Meanwhile, DFT calculations show that $*NH_2OH$ desorption is energetically favored over its reduction to NH_3 (Fig. 5f), enabling its coupling with $*CYC$ to form the oxime product. This spatial separation and enrichment effect at the interface enhances the C–N coupling selectivity.

Jia and co-workers reported a well-designed interfacial electrocatalytic system using an oxide-derived Cu catalyst for the synthesis of cyclohexanone oxime from phenol and hydroxylamine.[61] The Cu catalyst effectively balances the adsorption and activation of H_2O, phenol, and NH_2OH at the liquid–solid interface. Moderate adsorption of the *in situ*-formed cyclohexanone enables efficient coupling with NH_2OH, while suppressing its over-reduction to cyclohexanol (Fig. 5g). In addition, weak binding of the oxime product facilitates rapid desorption, avoiding further hydrogenation (Fig. 5h and i). These features enable a high FE (69.1%) and a phenol-to-oxime conversion rate of 97.5% at −0.9 V. In addition to its high selectivity and FE, this system demonstrated excellent practical applicability under industrially relevant conditions. Using a PEM flow cell at 50 mA cm^{-2}, the production rate of cyclohexanone oxime reached 54.0 g h^{-1} g$_{cat}^{-1}$ with a yield exceeding 90.0% and a carbon selectivity above 99.9%. The oxime product could be readily purified by simple separation and drying, affording an isolated yield of 99.9% with high purity (Fig. 5j).

Chen *et al.* proposed an interfacial regulation strategy based on the cooperative enrichment and coupling of key intermediates to enable the efficient aqueous electrosynthesis of oximes from NO_x and aldehyde substrates.[59] By tailoring the microenvironment at the Fe-based catalyst-electrolyte interface, this strategy facilitates the simultaneous surface accumulation and spatial proximity of NH_2OH and R-CHO, thereby promoting their preferential C–N coupling. The interfacial-specific enrichment of NH_2OH, combined with the strong adsorption of R-CHO (desorption energy increased by 23%), effectively suppresses the competing hydrogenation pathways. Moreover, the activation barrier for interfacial C–N coupling (0.32 eV) is significantly lower than that for NH_2OH reduction (0.68 eV), enabling a high oxime yield of up to 99%. In the subsequent flow reactor system, enhanced interfacial mass transport further boosts the oxime production rate to 22.8 g h^{-1} g$_{cat}^{-1}$.

Jia *et al.* engineered an MOF-derived Cu-Cu$_2$O heterojunction catalyst (Cu$_x$C$_y$O$_z$@600) for efficient hydroxylamine (HA) electrosynthesis *via in situ* electrochemical reconstruction.[29] In this structure, the cooperative interaction between Cu^0 and

Cu$^+$ at the interface optimizes the key steps in the reaction pathway, particularly facilitating the protonation and desorption of intermediates such as $*NO_2$ and $*NH_2OH$, respectively. The Cu(111)-Cu$_2$O(111) heterointerface plays a pivotal role in modulating the local electronic environment. This interface lowers the desorption energy of $*NH_2OH$ and facilitates the protonation of $*NO$ to $*NHO$ *via* a barrierless process, effectively overcoming the rate-determining step in HA formation. The coexistence of Cu^0 and Cu$^+$ species further promotes $*NO_2$ protonation and intermediate stabilization, enabling highly selective CP-O generation.

Shao *et al.* developed a scalable electrosynthetic system for converting methanol and ammonia into formamide *via* C–N coupling over a boron-doped diamond (BDD) electrode,[110] achieving an FE of 41.2% and selectivity of 73.2% at a current density of 120 mA cm^{-2}. The BDD electrode provides an inert liquid–solid interface that supports the oxidation of methanol to aldehyde-like species. Systematic tuning of the CH_3OH/NH_3 molar ratio and electrolyte pH demonstrated that modulating the local interfacial environment is key to enhancing the formamide selectivity and suppressing side reactions. The reaction pathway was further elucidated by analyzing the electrochemical behavior of model intermediates, where Fig. 5k confirms the oxidation of methanol to formaldehyde-like species as a prerequisite for C–N coupling.

Meng *et al.* developed a sustainable electrooxidation strategy to synthesize formamide under ambient conditions, offering an alternative to traditional high-temperature, high-pressure synthesis routes, achieving an FE of 40.39% and product selectivity of 74.26% under 100 mA cm^{-2} reaction conditions.[111] By employing a Pt electrocatalyst, particularly its oxidized α-PtO$_2$ surface phase, the system facilitates the formation and stabilization of aldehyde-like intermediates from methanol oxidation (Fig. 5l). These intermediates are subsequently attacked by ammonia through a nucleophilic pathway to generate formamide. The spatial confinement and reactive environment at the electrode–electrolyte interface effectively direct the multi-step conversion and suppress overoxidation, underscoring the vital role of interface engineering in modulating the C–N coupling efficiency.

3.4 Dual-site synergy

Single active sites may not be sufficient to perform multi-substrate complex reactions involving both NO_x and carbon-containing species. In contrast, dual-site catalysts, which contain two types of active centers with different functions, can offer new active sites to facilitate the adsorption/activation/conversion of different substrates. For example, site A to active NO_x, while site B to active carbon-containing species. The close distance between these sites can help transfer key intermediates and encourage the formation of C–N bonds. This cooperative mechanism is useful for improving both the activity and selectivity. Therefore, dual-site catalyst design has become a promising strategy for the construction of more efficient NO_x-involved C–N coupling reactions.

This journal is © the Partner Organisations 2025

*Inorg. Chem. Front.*, 2025, **12**, 6926–6945 | **6935**

As a typical example of dual-site catalysis, Xian *et al.* constructed a CoFe alloy-decorated self-standing carbon fiber membrane (CoFe-SSM), which promoted the electrosynthesis of α-amino acids from NO and α-keto acids *via* a dual-site synergy strategy.[112] In this system, the CoFe alloy provides two distinct but synergistic metal centers, where the Co sites facilitated the reduction of NO to hydroxylamine (NH_2OH), while the Fe sites assisted in the transformation of the oxime intermediates into α-keto acids *via* hydrogenation. This dual-site synergy strategy led to improved C–N coupling selectivity and FE compared to single-site catalyst systems (Fig. 6a).

Liao *et al.* developed a Cu–Bi bimetallic catalyst derived from MOF arrays grown on copper foam (Cu/Bi-C@CF), which enabled the high-efficiency electrosynthesis of glycine from nitrate and glyoxylate under ambient conditions.[97] Cu and Bi act as two functionally distinct but spatially adjacent active sites, where Cu reduces nitrate to hydroxylamine (NH_2OH), while Bi modulates the local electronic environment of Cu, weakening *NO adsorption and enhancing NH_2OH desorption. XPS and XANES data show electron transfer from Bi to Cu, weakening excessive *NO adsorption and enhancing the NH_2OH selectivity. *In situ* ATR-FTIR spectra (Fig. 6b) show the formation of C=N-OH and CH_2 groups, supporting oxime formation and subsequent hydrogenation. Compared with monometallic Cu or Bi catalysts, the Cu–Bi system demonstrates significantly improved FE and product selectivity, confirming the importance of dual-site synergy in directing the C–N coupling pathway.

Wu and co-workers developed a PdCu nano-bead-wire (Pd_1Cu_1 NBWs) catalyst that exhibits a dual-site synergy in catalyzing the tandem coupling of biomass-derived pyruvic acid (PA) and nitrate (NO_3^-) into alanine.[79] The reaction proceeds
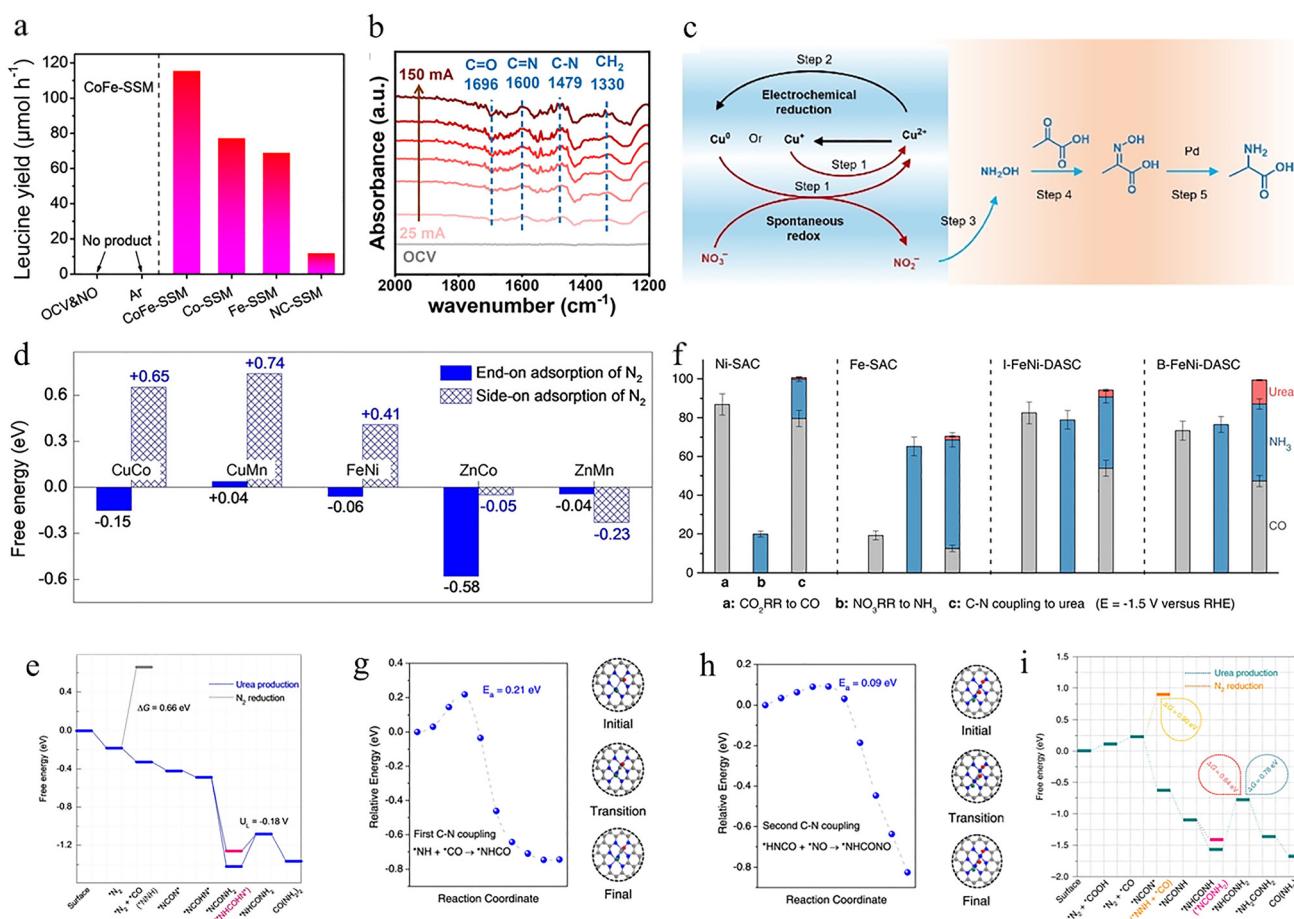
Fig. 6 (a) Comparative leucine production yields of the CoFe-SSM catalyst and control samples under varying reaction conditions.[112] Reproduced with permission from ref. 112, Copyright © 2023, Wiley-VCH GmbH. (b) *In situ* ATR-FTIR spectra of the electrosynthesis of glycine on Cu/Bi-C@CF.[97] Reproduced with permission from ref. 97, Copyright © 2024, Wiley-VCH GmbH. (c) Mechanism of the nitrate and glyoxylate C–N coupling reaction.[79] Reproduced with permission from ref. 79, Copyright © 2023, Wiley-VCH GmbH. (d) Comparison of free energies for side-on *versus* end-on N_2 adsorption on diatomic catalysts.[113] (e) Energy barrier of C–N coupling on ZnMn-N, Cl.[113] Reproduced with permission from ref. 113, Copyright © 2023, Wiley-VCH GmbH. (f) Comparative analysis on Ni-SAC, Fe-SAC, I-FeNi-DASC, and B-FeNi-DASC catalysts at −1.4 V *vs.* RHE.[114] (g) Pathway for the first C–N coupling forming *NHCO intermediate.[114] (h) Pathway for the second C–N coupling forming *NHCONO intermediate.[114] Reproduced with permission from, ref. 114 Copyright © 2022, Springer Nature. (i) Reaction pathway of Pd_1Cu_1/TiO_2-400.[57] Reproduced with permission from ref. 57, Copyright © 2020, Springer Nature.

6936 | *Inorg. Chem. Front.*, 2025, **12**, 6926–6945

This journal is © the Partner Organisations 2025

through a three-step electrochemical-chemical-electrochemical cascade mechanism. Initially, the Cu sites catalyze the reduction of nitrate to hydroxylamine (NH_2OH), serving as the nitrogen donor. Subsequently, NH_2OH spontaneously condenses with PA to form a pyruvic oxime intermediate. Finally, the Pd sites drive the electrochemical hydrogenation of the oxime to produce alanine as the main product (Fig. 6c). By spatially separating the activation of nitrate and the reduction of the C=N intermediate, this dual-site system enables precise control over individual reaction steps. As a result, a high alanine yield of 54.8% is achieved under ambient conditions, significantly suppressing the formation of side products such as lactic acid.

Zhang et al. achieved 63.5% FE urea electrosynthesis via Zn–Mn dual-site synergy with axial Cl coordination (ZnMn-N, Cl).[113] By leveraging the complementary electronic characteristics of Zn and Mn, the catalyst forms local electrophilic and nucleophilic centers that enable the co-adsorption and co-activation of CO_2 and N_2 molecules. This spatial and electronic cooperation facilitates a one-step C–N coupling pathway, bypassing the formation of ammonia intermediates, and achieving a nearly 100% N-selectivity and a maximum FE of 63.5% under CO pre-poisoning. The N_2 molecule adopts a side-on adsorption mode on the Zn–Mn pair, which is thermodynamically more favorable than the conventional end-on con-

figuration. The subsequent coupling with *CO species derived from CO_2 reduction directly forms an *NCON* intermediate (Fig. 6d and e).

Zhang et al. developed a bonded Fe–Ni diatomic electrocatalyst (B-FeNi-DASC) to achieve synergistic urea synthesis (Fig. 6f).[114] By integrating Fe and Ni atoms into a well-defined diatomic configuration, this catalyst achieves the concurrent adsorption and activation of nitrate and CO_2, offering spatial proximity and electronic complementarity between the two active centers. Compared to single-atom and non-bonded diatomic systems, the bonded Fe–Ni sites not only generate abundant *NO and *CO intermediates but also directly participate in the C–N bond formation steps (Fig. 6g and h).

Chen and co-workers developed a dual-site synergy strategy by anchoring PdCu alloy nanoparticles onto oxygen-vacancy-rich TiO_2 nanosheets (Pd_1Cu_1/TiO_2-400), enabling the electrocatalytic coupling of N_2 and CO_2 to produce urea under ambient conditions.[57] In this catalyst system, Pd enhances back-donation to weaken the N≡N bond of N_2, while Cu facilitates CO_2 activation and *CO intermediate stabilization. On the PdCu alloy surface, the activated *N=N* species couples with CO to form the key intermediate *NCON*, which proceeds through a kinetically favorable (E_a = 0.79 eV) and thermodynamically downhill (ΔG = −0.89 eV) pathway (Fig. 6i).
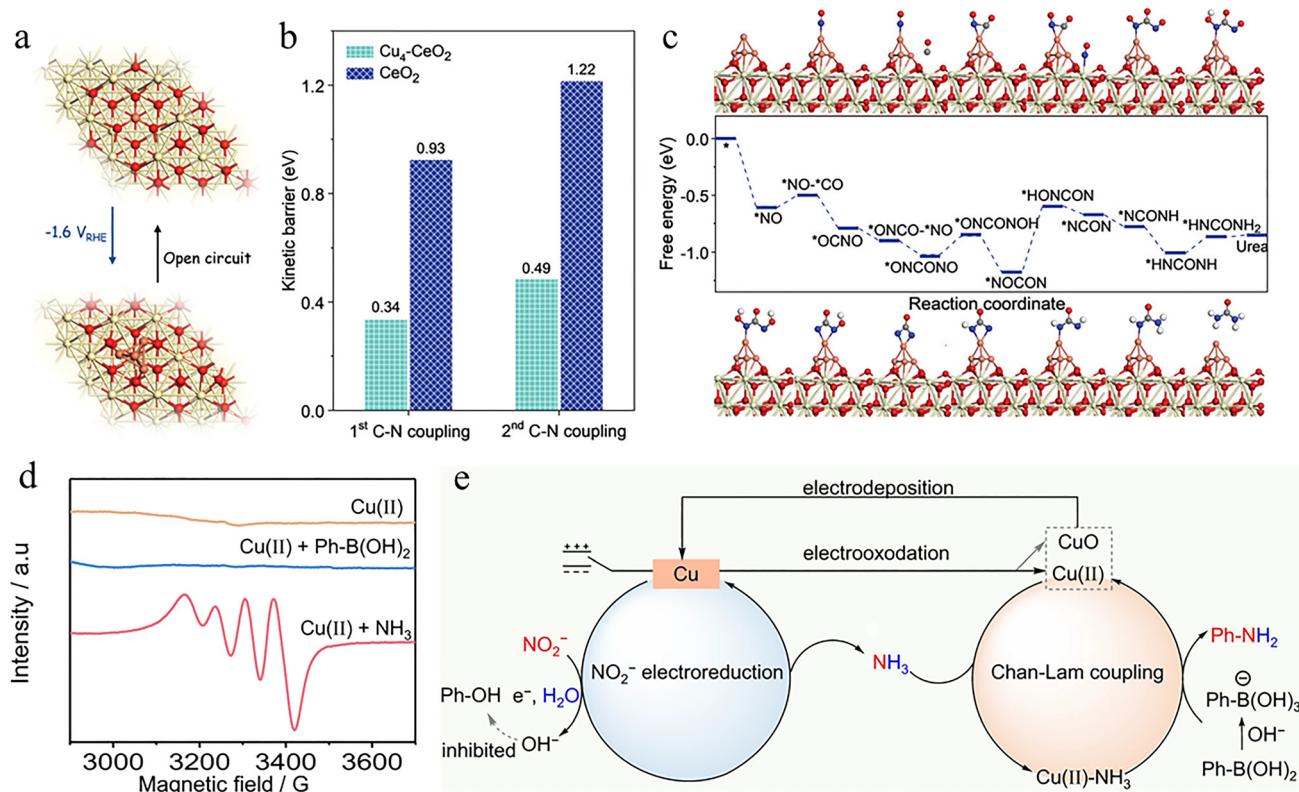
Fig. 7 (a) Free energy changes of urea production on Pd_1Cu_1/TiO_2-400.[94] (b) Kinetic barriers of *OCNO and *ONCONO on CeO_2 vs. Cu_4-CeO_2.[94] (c) Free-energy profiles and optimized geometry of C–N coupling on Cu_4-CeO_2.[94] Reproduced with permission from ref. 94, Copyright © 2023, Wiley-VCH GmbH. (d) EPR spectrum of Cu(II)-NH_3.[98] (e) Catalytic mechanism.[98] Reproduced with permission from ref. 98, Copyright © 2023, Springer Nature.

This journal is © the Partner Organisations 2025

Inorg. Chem. Front., 2025, **12**, 6926–6945 | **6937**
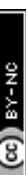
Table 1 Progress summary of C–N coupling reactions

Regulation strategy	Catalyst	Production	Electrolyte	Condition	Selectivity	Conversion	FE	Yield	Ref.
Defect engineering	AD-Fe/NC	Amino acids	0.1 M HCl + 20 mM 3-methyl-2-oxobutanoic acid	−0.6 V vs. RHE	11.3%	47.4%	9.5%	32.1 μmol mg$_{cat}^{-1}$	60
Defect engineering	Pd/Cu-V$_{Cu}$	DMF	0.5 M KHCO$_3$	20 mA cm^{-2}	—	—	37.5%	385 mmol h^{-1} g$_{cat}^{-1}$	99
Defect engineering	e-OD-Cu	HMTA	0.1 M KOH + 0.5 M K$_2$SO$_4$	−0.3 V vs. RHE	99%	—	74.9%	76.8%	100
Defect engineering	Cu/PI-X	Urea	0.1 M KHCO$_3$ + 0.1 M KNO$_3$	−1.4 V vs. RHE	—	—	14.3%	255.0 mmol h^{-1} g^{-1}	101
Defect engineering	V$_o$-CeO$_2$-750	Urea	0.1 M KHCO$_3$ + 50 mM KNO$_3$	−1.6 V vs. RHE	—	—	—	943.6 mg h^{-1} g^{-1}	102
Defect engineering	ReMn-NC	Urea	PBS	−0.3 V vs. RHE	89.1%	—	—	48.9 ± 2.4 mg g^{-1} h^{-1}	103
Defect engineering	Cu$_{0.7}$In$_3$-C	Urea	0.1 M KHCO$_3$	−1.5 V vs. RHE	—	—	—	13.1 mmol g^{-1} h^{-1}	62
Defect engineering	NS-CNS	Alanine	1.0 M KOH	−0.5 V vs. RHE	>99.9%	>75%	79.5%	1199 μmol h^{-1} cm^{-2}	104
Coordination environment design	ZIF-7/CGF	1-PDO	0.1 M KOH	−0.1 V vs. RHE	—	—	75.9%	73.1%	43
Coordination environment design	Cu-S	Cyclohexanone oxime	0.5 M PBS + 0.2 mM CYC + 2 mM NaNO$_2$	−0.9 V vs. Ag/AgCl	99%	—	26%	92%	42
Coordination environment design	HEA-PdCuAgBiInene	Cyclohexanone oxime	0.5 M PBS + 0.02 M CYC + 0.1 M KNO$_2$	−0.9 V vs. Ag/AgCl	—	—	47.6%	~100%	95
Coordination environment design	NH$_2$-MIL-53(Al)	2-Pyridinealdoxime	0.1 M KOH	13 mA	—	—	49.8%	92.1%	105
Coordination environment design	MgO-SCM	4-CBOE	0.001 M KOH/0.05 M Li$_2$SO$_4$	12 mA	93%	—	65.1%	94%	106
Coordination environment Design coordination	adFe-TiO$_x$/Ti	Glycine	0.5 M H$_2$SO$_4$ + 0.1 M GA + 1.0 M NaNO$_3$	−0.7 V vs. RHE	80.2%	100%	80.5%	83.4%	107
Coordination environment design	OD-Ag	Alanine	0.5 M PBS	−0.56 V vs. RHE	—	—	17.0%	11.45 mmol h^{-1} g^{-1}	47
Coordination environment design	CuPc-amino	Urea	0.1 M KHCO$_3$ + 0.05 M KNO$_3$	−1.6 V vs. RHE	—	—	11.9 ± 0.6%	103.1 ± 5.3 mmol h^{-1} g^{-1}	108
Interface engineering	Ag-50	Cyclohexanone oxime	0.5 M Na$_2$CO$_3$ + 0.5 M NaNO$_2$	100 mA cm^{-2}	—	99.6%	83.8%	0.78 mmol h^{-1} cm^{-2}	44
Interface engineering	Fe	Cyclohexanone oxime	0.5 M K$_2$CO$_3$ + 1 M KNO$_3$	500 mA cm^{-2}	100%	100%	~100%	59.5 g h^{-1} g$_{cat}^{-1}$	78
Interface engineering	Cu	Cyclohexanone oxime	0.5 M KHCO$_3$ + 20 mM phenol + 10 mM (NH$_3$OH)$_2$SO$_4$	−0.9 V vs. RHE	94%	97.5%	69.1%	90%	61
Interface engineering	Fe-based	Benzaldoxime	0.5 M H$_2$SO$_4$ + 0.5 M K$_2$CO$_3$	200 mA cm^{-2}	—	—	1.52%	99%	59
Interface engineering	Cu$_x$C$_y$O$_z$@600	CP-O	0.5 M KNO$_3$ + 0.1 M CP	−1.6 V vs. Ag/AgCl	96.2%	99%	47.8%	34.9 mg h^{-1} cm^{-2}	29
Interface engineering	BDD	Formamide	0.5 M NaHCO$_3$	120 mA cm^{-2}	73.2%	—	41.2%	461.39 μmol cm^{-2} h^{-1}	110
Interface engineering	Pt	Formamide	0.5 M NaHCO$_3$/0.25 M H$_2$SO$_4$	100 mA cm^{-2}	74.26%	—	40.39%	305.4 μmol cm^{-2} h^{-1}	111
Dual-site synergy	CoFe-SSM	α-Amino acids	0.1 M HCl	−0.7 V vs. RHE	56.7%	98.5%	32.4%	115.4 μmol h^{-1}	112
Dual-site synergy	Cu/Bi–C@CF	Glycine	0.1 M HCl	75 mA	89%	>99%	65.9%	89%	97
Dual-site synergy	Pd$_1$Cu$_1$ NBWs	Alanine	1.0 M KNO$_3$ + 50 mM PA	−0.3 V vs. RHE	—	—	—	54.8%	79
Dual-site synergy	ZnMn-N	Urea	KHCO$_3$	−0.3 V vs. RHE	100%	—	63.5%	4.0 mmol g^{-1} h^{-1}	113
Dual-site synergy	B-FeNi-DASC	Urea	0.1 M KHCO$_3$ + 50 mM KNO$_3$/KNO$_2$	−1.5 V vs. RHE	—	—	17.8%	20.2 mmol h^{-1} g^{-1}	114
Dual-site synergy	Pd$_1$Cu$_1$/TiO$_2$-400	Urea	0.1 M KHCO$_3$	−0.4 V vs. RHE	—	—	8.92%	3.36 mmol g^{-1} h^{-1}	57
Emerging architectures	Cu$_1$-CeO$_2$	Urea	0.1 M KHCO$_3$ + 50 mM KNO$_3$	−1.6 V vs. RHE	—	—	—	52.84 mmol h^{-1} g$_{cat}^{-1}$	94
Emerging architectures	LC-Cu NC	Arylamines	0.25 M PBS + MeOH	E_{ca} = −1.1 V, E_{an} = 0.4 V	—	—	95%	72%	98
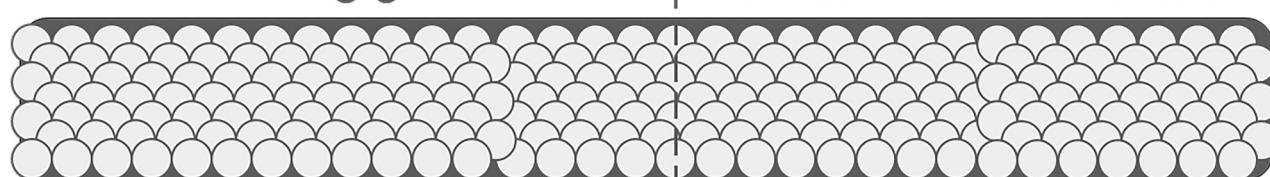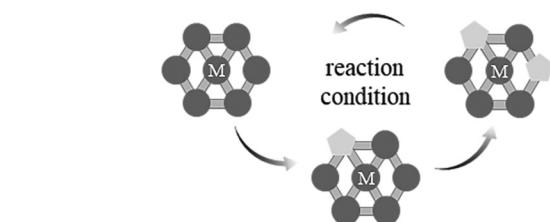
6938 | *Inorg. Chem. Front.*, 2025, **12**, 6926–6945

This journal is © the Partner Organisations 2025
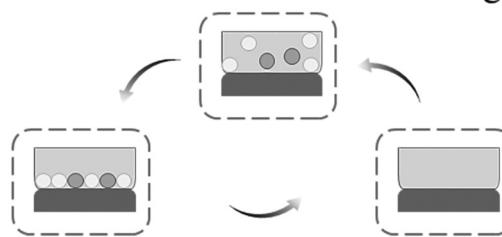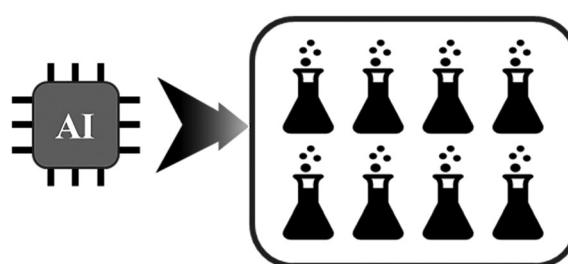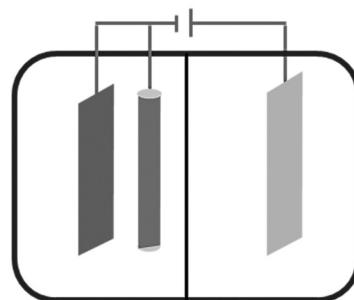
Fig. 8 Four strategic directions for promoting electrocatalytic C–N bond formation. The schematic outlines the strategies integrated across four dimensions to address the ongoing challenges in the electrocatalytic C–N bond formation process. (a) Dynamic structural adaptability. (b) Regulation of the reaction microenvironment to inhibit competing reactions. (c) Application of artificial intelligence and machine learning for high-throughput catalyst screening and mechanism simulation. (d) Modular flow reactors, providing a foundation for achieving industrial-scale application.

3.5 Emerging architectures

In addition to conventional catalyst systems, emerging architectures have been developed to address the growing complexity of selective C–N coupling reactions. These include dynamically evolving structures, spatiotemporally modulated systems, and hybrid electrolyte-catalyst interfaces. Unlike the four aforementioned categories, which primarily focus on spatially static structural modifications such as defect engineering, coordination tuning, interfacial design, and dual-site synergy, emerging architectures emphasize dynamic, adaptive, and process-coupled catalyst behavior. This shift reflects a transition from material-centric design principles to those that are responsive to the reaction environment.

Wei *et al.* developed a dynamic reconstruction strategy by designing Cu_1 single atoms supported on CeO_2 (Cu_1-CeO_2), which undergo reversible structural transformation into Cu_4 clusters under electrocatalytic conditions.[94] This dynamic evolution bridges single-atom precision with cluster-level activity, enabling a self-adjusting catalytic configuration that adapts to

the electrochemical environment. The reconstituted Cu_4 clusters act as real active sites (Fig. 7a), significantly enhancing the simultaneous adsorption and activation of NO_3^- and CO_2. DFT calculations reveal that the C–N coupling proceeds *via* the Eley–Rideal mechanism, where *NO and *CO form the key intermediate *OCNO with a low energy barrier of 0.34 eV on Cu_4-CeO_2, which is significantly lower than the 0.93 eV required on pristine CeO_2 (Fig. 7b and c). Subsequent coupling with a second *NO yields *ONCONO, which undergoes eight electron–proton-transfer steps to produce urea.

He *et al.* demonstrated that pulse-engineered spatiotemporal control fundamentally transforms electrocatalytic arylamine synthesis by dynamically orchestrating three synchronized processes,[98] as follows: (1) during cathodic pulses (−1.1 V), low-coordinated Cu nanocorals leverage undercoordinated sites (CN = 9.75) to reduce NO_2^- to NH_3 with 95% FE, accumulating critical nitrogen feedstock. (2) Switching to anodic pulses (+0.4 V) oxidizes the Cu electrode to solubilize catalytic Cu(II), which coordinates with NH_3 to form the key Cu(II)-NH_3 intermediate (Fig. 7d), while simultaneously driving the elec-

trophoretic migration of the nucleophilic $ArB(OH)_3^-$ toward the anode and consuming OH^- ions *via* Cu oxidation ($2Cu + 2OH^- \rightarrow Cu_2O + H_2O$), thereby suppressing phenol byproducts from 28% to <5% (Fig. 7e). (3) The rapid polarity alternation maintains high local concentrations of $Cu(\text{II})/NH_3$ near the electrode surface, accelerating C–N bond formation to achieve 72% arylamine yield (an 8-fold enhancement over static potential methods). This temporal strategy further enables the self-regeneration of the catalytic Cu species through cathodic electrodeposition and can be expanded to ^{15}N-labeled arylamine synthesis (98.99% isotopic purity) and click reactions, establishing pulsed electrochemistry as a paradigm-shifting approach for complex organic electrosynthesis beyond static catalyst design.

4 Conclusions and outlook

In this paper, we have systematically reviewed the recent progress in electrocatalytic C–N coupling reactions involving NO_x species and various carbon-based reactants (Table 1). By integrating NO_x species with diverse carbon sources (such as CO_2, aldehydes, and biomass derivatives), these C–N coupling reactions offer a sustainable route to synthesize high-value nitrogen-containing products, including oximes, amines, amides, amino acids, and urea.

Focusing on the underlying catalytic mechanisms and structural-function correlations, we classified the catalyst engineering strategies into five representative categories including defect engineering, coordination environment design, interface engineering, dual-site synergy, and emerging architectures. These approaches address key challenges such as poor intermediate stability, weak substrate adsorption compatibility, and low selectivity.

Despite the substantial progress enabled by the five major catalyst design strategies, several fundamental challenges remain unresolved. For instance, the underlying reaction kinetics and the behavior of the transient intermediates under the dynamic electrochemical environment are still not clearly understood, making it difficult to rationally modulate activity and selectivity. Competing reactions such as hydrogen evolution, over-reduction and other undesired side reactions often interfere with the desired coupling steps. To further push the frontiers of NO_x-involved C–N electrosynthesis, we propose four strategic development directions (Fig. 8).

4.1 Dynamic structural adaptability

Conventional static catalyst structures are often insufficient for accommodating the dynamic evolution of the active sites during multi-step C–N coupling (Fig. 8a). Future efforts should focus on the development of adaptive catalytic systems capable of reversible reconstruction, single-atom to cluster transitions, or self-regulated site reconfiguration in response to the reaction environment. These dynamic architectures can provide spatiotemporal modulation of the activity and selectivity across complex reaction pathways.

4.2 Reaction microenvironment regulation

The rational design of interfacial microenvironments, including local pH, reactant gradients, phase interfaces (*e.g.*, solid–liquid–gas), and electric field distribution, is critical for steering intermediate adsorption and suppressing competing pathways (Fig. 8b). Engineering spatially confined or hydrophilic/hydrophobic domains on catalyst surfaces can selectively enrich the reactants, promote intermediate pairing, and improve mass transport for enhanced C–N bond formation.

4.3 AI and machine learning

Artificial intelligence (AI) and machine learning (ML) are expected to play increasingly important roles in catalyst development (Fig. 8c). By integrating large-scale experimental and theoretical databases, ML algorithms can accelerate the identification of performance descriptors, predict reaction energetics, and guide the inverse design of catalysts with tailored electronic structures and adsorption characteristics. Coupling AI with high-throughput screening and automated synthesis platforms will enable more efficient exploration of the vast catalyst space.

4.4 High-efficient reactor design

To realize the practical deployment of electrocatalytic C–N coupling systems, efforts should be directed toward the design of scalable and modular electrochemical flow reactors (Fig. 8d). These systems can provide precise control over the reaction residence time, electrode configuration, and mass transfer conditions, while facilitating continuous production and system integration. The combination of optimized catalysts with intelligent flow designs can bridge the gap between laboratory demonstrations and industrial applications.

In summary, electrocatalytic NO_x-involved C–N coupling represents a promising frontier in green chemical synthesis. Through advances in dynamic catalyst design, microenvironment control, AI-assisted optimization, and scalable system engineering, the field is poised to overcome current limitations and move toward high-efficiency, selective, and industrially viable electrosynthesis platforms. Future progress will rely on the integration of scalable catalyst design with modular reactor engineering, as well as cross-disciplinary collaboration spanning materials science, artificial intelligence, and process systems. Addressing these bottlenecks will be essential for translating NO_x-involved electrosynthesis from conceptual frameworks into practical, sustainable applications.

Author contributions

R. W., X. S. and B. H. wrote the manuscript. X. S. and B. H. supervised the project.

Conflicts of interest

The authors have no conflicts of interest to declare.

6940 | *Inorg. Chem. Front.*, 2025, **12**, 6926–6945

This journal is © the Partner Organisations 2025

Data availability

No primary research results, software or code has been included and no new data were generated or analysed as part of this review.

Acknowledgements

References

1 M. He, Y. Sun and B. Han, Green Carbon Science: Efficient Carbon Resource Processing, Utilization, and Recycling towards Carbon Neutrality, *Angew. Chem., Int. Ed.*, 2022, **61**, e202112835.

2 P. Gao, L. Zhong, B. Han, M. He and Y. Sun, Green Carbon Science: Keeping the Pace in Practice, *Angew. Chem., Int. Ed.*, 2022, **61**, e202210095.

3 M. He, Y. Sun and B. Han, Green Carbon Science: Scientific Basis for Integrating Carbon Resource Processing, Utilization, and Recycling, *Angew. Chem., Int. Ed.*, 2013, **52**, 9620–9633.

4 P. De Luna, C. Hahn, D. Higgins, S. A. Jaffer, T. F. Jaramillo and E. H. Sargent, What would it take for renewably powered electrosynthesis to displace petrochemical processes?, *Science*, 2019, **364**, eaav3506.

5 A. Majumdar and J. Deutch, Research Opportunities for CO2 Utilization and Negative Emissions at the Gigatonne Scale, *Joule*, 2018, **2**, 805–809.

6 J. Li, Y. Zhang, K. Kuruvinashetti and N. Kornienko, Construction of C–N bonds from small-molecule precursors through heterogeneous electrocatalysis, *Nat. Rev. Chem.*, 2022, **6**, 303–319.

7 V. R. Stamenkovic, D. Strmcnik, P. P. Lopes and N. M. Markovic, Energy and fuels from electrochemical interfaces, *Nat. Mater.*, 2017, **16**, 57–69.

8 A. A. Peterson and J. K. Nørskov, Activity Descriptors for CO2 Electroreduction to Methane on Transition-Metal Catalysts, *J. Phys. Chem. Lett.*, 2012, **3**, 251–258.

9 S. Jia, L. Wu, H. Liu, R. Wang, X. Sun and B. Han, Nitrogenous Intermediates in NOx-involved Electrocatalytic Reactions, *Angew. Chem., Int. Ed.*, 2024, **63**, e202400033.

10 S. Song, V. Yuen, L. Di, Q. Sun, K. Zhou and N. Yan, Integrating Biomass into the Organonitrogen Chemical Supply Chain: Production of Pyrrole and d-Proline from Furfural, *Angew. Chem., Int. Ed.*, 2020, **59**, 19846–19850.

11 Y. Wan, M. Zheng, W. Yan, J. Zhang and R. Lv, Fundamentals and Rational Design of Heterogeneous C-N Coupling Electrocatalysts for Urea Synthesis at Ambient Conditions, *Adv. Energy Mater.*, 2024, **14**, 2303588.

12 L. Zhang, X. Sun and B. Han, Electrocatalytic CO2 reduction to a single multi-carbon product, *Sci. Bull.*, 2024, **69**, 563–565.

13 G. Xie, W. Guo, Z. Fang, Z. Duan, X. Lang, D. Liu, G. Mei, Y. Zhai, X. Sun and X. Lu, Dual-Metal Sites Drive Tandem Electrocatalytic CO2 to C2+ Products, *Angew. Chem., Int. Ed.*, 2024, **63**, e202412568.

14 Y. Guo, N. Sun, L. Luo, X. Cheng, X. Chen, X. Yan, S. Shen and J. Zhang, Potential-dependent insights into the origin of high ammonia yield rate on copper surface via nitrate reduction: A computational and experimental study, *J. Energy Chem.*, 2024, **96**, 272–281.

15 J. G. Chen, R. M. Crooks, L. C. Seefeldt, K. L. Bren, R. M. Bullock, M. Y. Darensbourg, P. L. Holland, B. Hoffman, M. J. Janik, A. K. Jones, M. G. Kanatzidis, P. King, K. M. Lancaster, S. V. Lymar, P. Pfromm, W. F. Schneider and R. R. Schrock, Beyond fossil fuel–driven nitrogen transformations, *Science*, 2018, **360**, eaar6611.

16 L. Lin, P. Su, Y. Han, Y. Xu, Q. Ni, X. Zhang, P. Xiong, Z. Sun, G. Sun and X. Chen, Advances in regulating the electron spin effect toward electrocatalysis applications, *eScience*, 2025, **5**, 100264.

17 Y. Wang, P. Zhang, X. Lin, G. Zhang, H. Gao, Q. Wang, Z.-J. Zhao, T. Wang and J. Gong, Wide-pH-range adaptable ammonia electrosynthesis from nitrate on Cu-Pd interfaces, *Sci. China:Chem.*, 2023, **66**, 913–922.

18 L. Zhang, J. Feng, R. Wang, L. Wu, X. Song, X. Jin, X. Tan, S. Jia, X. Ma, L. Jing, Q. Zhu, X. Kang, J. Zhang, X. Sun and B. Han, Switching CO-to-Acetate Electroreduction on Cu Atomic Ensembles, *J. Am. Chem. Soc.*, 2025, **147**, 713–724.

19 L. Wu, L. Zhang, J. Feng, S. Jia, R. Wang, X. Song, X. Ma, Q. Zhu, X. Kang, Q. Qian, X. Sun and B. Han, Intermittent electrolysis enabling the enhanced efficiency and stability for nitrate reduction, *Chem*, 2025, **11**, 102591.

20 J. Feng, L. Wu, S. Liu, L. Xu, X. Song, L. Zhang, Q. Zhu, X. Kang, X. Sun and B. Han, Improving CO2-to-C2+ Product Electroreduction Efficiency via Atomic Lanthanide Dopant-Induced Tensile-Strained CuOx Catalysts, *J. Am. Chem. Soc.*, 2023, **145**, 9857–9866.

21 L. Zhang, J. Feng, L. Wu, X. Ma, X. Song, S. Jia, X. Tan, X. Jin, Q. Zhu, X. Kang, J. Ma, Q. Qian, L. Zheng, X. Sun and B. Han, Oxophilicity-Controlled CO2 Electroreduction to C2+ Alcohols over Lewis Acid Metal-Doped Cuδ+ Catalysts, *J. Am. Chem. Soc.*, 2023, **145**, 21945–21954.

22 J. Wang, Z. Yao, L. Hao and Z. Sun, Electrocatalytic coupling of CO2 and N2 for urea synthesis, *Curr. Opin. Green Sustainable Chem.*, 2022, **37**, 100648.

23 M. T. Sabatini, L. T. Boulton, H. F. Sneddon and T. D. Sheppard, A green chemistry perspective on catalytic amide bond formation, *Nat. Catal.*, 2019, **2**, 10–17.

This journal is © the Partner Organisations 2025

Inorg. Chem. Front., 2025, **12**, 6926–6945 | **6941**

24 S. Kuang, T. Xiao, H. Chi, J. Liu, C. Mu, H. Liu, S. Wang, Y. Yu, T. J. Meyer, S. Zhang and X. Ma, Acetamide Electrosynthesis from CO2 and Nitrite in Water, *Angew. Chem., Int. Ed.*, 2024, **63**, e202316772.

25 X. Qi, Y. Zhang, C. Chen, J. Yang, J. Wen, Z. Zhuang, Z. Zhang, D. Wang and H. Zhang, Deciphering the N-N Coupling Mechanism Over Iron-Copper Alloy Catalysts During Ammonia Decomposition, *Angew. Chem., Int. Ed.*, 2025, e202509322.

26 S. Zhu, H. Zhang, B. Sun, Z. Bai, G. He, G. Chen and H. Wang, Nitrene-mediated aminative N-N-N coupling: facile access to triazene 1-oxides, *Chem. Sci.*, 2025, **16**, 6458–6467.

27 Y. Guan, Y. Li, Z. Li, Y. Hou, L. Lei and B. Yang, Promotion of C-C Coupling in the CO2 Electrochemical Reduction to Valuable C2+ Products: From Micro-Foundation to Macro-Application, *Adv. Mater.*, 2025, **37**, 2417567.

28 S. Jia, L. Zhang, H. Liu, R. Wang, X. Jin, L. Wu, X. Song, X. Tan, X. Ma, J. Feng, Q. Zhu, X. Kang, Q. Qian, X. Sun and B. Han, Upgrading of nitrate to hydrazine through cascading electrocatalytic ammonia production with controllable N-N coupling, *Nat. Commun.*, 2024, **15**, 8567.

29 S. Jia, L. Wu, X. Tan, J. Feng, X. Ma, L. Zhang, X. Song, L. Xu, Q. Zhu, X. Kang, X. Sun and B. Han, Synthesis of Hydroxylamine via Ketone-Mediated Nitrate Electroreduction, *J. Am. Chem. Soc.*, 2024, **146**, 10934–10942.

30 J. Feng, L. Wu, X. Song, L. Zhang, S. Jia, X. Ma, X. Tan, X. Kang, Q. Zhu, X. Sun and B. Han, CO2 electrolysis to multi-carbon products in strong acid at ampere-current levels on La-Cu spheres with channels, *Nat. Commun.*, 2024, **15**, 4821.

31 X. Song, X. Ma, T. Chen, L. Xu, J. Feng, L. Wu, S. Jia, L. Zhang, X. Tan, R. Wang, C. Chen, J. Ma, Q. Zhu, X. Kang, X. Sun and B. Han, Urea Synthesis via Coelectrolysis of CO2 and Nitrate over Heterostructured Cu-Bi Catalysts, *J. Am. Chem. Soc.*, 2024, **146**, 25813–25823.

32 P. Liao, J. Kang, R. Xiang, S. Wang and G. Li, Electrocatalytic Systems for NOx Valorization in Organonitrogen Synthesis, *Angew. Chem., Int. Ed.*, 2024, **63**, e202311752.

33 Y. Zeng, C. Priest, G. Wang and G. Wu, Restoring the Nitrogen Cycle by Electrochemical Reduction of Nitrate: Progress and Prospects, *Small Methods*, 2020, **4**, 2000672.

34 B. H. Ko, B. Hasa, H. Shin, Y. Zhao and F. Jiao, Electrochemical Reduction of Gaseous Nitrogen Oxides on Transition Metals at Ambient Conditions, *J. Am. Chem. Soc.*, 2022, **144**, 1258–1266.

35 J. Zhou, S. Han, R. Yang, T. Li, W. Li, Y. Wang, Y. Yu and B. Zhang, Linear Adsorption Enables NO Selective Electroreduction to Hydroxylamine on Single Co Sites, *Angew. Chem., Int. Ed.*, 2023, **62**, e202305184.

36 R. Wang, S. Jia, L. Wu, L. Zhang, X. Song, X. Tan, C. Zheng, W. Li, X. Ma, Q. Qian, X. Kang, Q. Zhu, X. Sun

and B. Han, Tuning the Acid Hardness Nature of Cu Catalyst for Selective Nitrate-to-Ammonia Electroreduction, *Angew. Chem., Int. Ed.*, 2025, **64**, e202425262.

37 J. Tan, Q. Shen, X. Jin, M. Wang, B. A. W. Chen, Z. Wei, L. Zhang and J. Shi, Dual Active Sites on Cu/Cu2O Heterostructures for the Cascade Electrocatalytic Synthesis of Amino Acids, *J. Am. Chem. Soc.*, 2025, **147**, 23635–23642.

38 C. Zhao, Y. Jin, J. Yuan, Q. Hou, H. Li, X. Yan, H. Ou and G. Yang, Tailoring Activation Intermediates of CO2 Initiates C–N Coupling for Highly Selective Urea Electrosynthesis, *J. Am. Chem. Soc.*, 2025, **147**, 8871–8880.

39 C. L. Rooney, Q. Sun, B. Shang and H. Wang, Electrocatalytic Reductive Amination of Aldehydes and Ketones with Aqueous Nitrite, *J. Am. Chem. Soc.*, 2025, **147**, 9378–9385.

40 Y. Wang, S. Xia, K. Chen, J. Zhang, C. Yu, J. Wu, P. Wang, W. Zhang and Y. Wu, Balancing Intermediates Formation on Atomically Pd-Bridged Cu/Cu2O Interfaces for Kinetics-Matching Electrocatalytic C–N Coupling Reaction, *Angew. Chem., Int. Ed.*, 2025, **64**, e202503011.

41 H. Liu, S. Jia, L. Wu, R. Wang, L. Zhang, X. Song, X. Tan, X. Ma, X. Jin, H. Guo, X. Sui, Q. Li, R. Feng, L. Jing, Q. Qian, J. Zhang, L. He, X. Sun and B. Han, Circumventing Scaling Relations via Gradient Orbital Coupling Promotes Ammonia Electrosynthesis on Cobalt Catalyst, *Angew. Chem., Int. Ed.*, 2025, e202510478.

42 Y. Wu, J. Zhao, C. Wang, T. Li, B.-H. Zhao, Z. Song, C. Liu and B. Zhang, Electrosynthesis of a nylon-6 precursor from cyclohexanone and nitrite under ambient conditions, *Nat. Commun.*, 2023, **14**, 3057.

43 J. Kang, P. Liao, R. Xiang, W. Liao, C. Yang, S. Wang, Q. Liu and G. Li, Interfacial Asymmetrically Coordinated Zn-MOF for High-Efficiency Electrosynthetic Oxime, *Angew. Chem., Int. Ed.*, 2025, **64**, e202419550.

44 F. Zhang, Q.-Y. Fan, Y.-C. Huang, H. Li, H. Zou, Y. Li, Y. Zou, S. Wang, C. Yang, Y. Lu and H. Yang, A Pickering-emulsion-droplet-integrated electrode for the continuous-flow electrosynthesis of oximes, *Nat. Synth.*, 2025, **4**, 479–487.

45 G. Evano, N. Blanchard and M. Toumi, Copper-Mediated Coupling Reactions and Their Applications in Natural Products and Designed Biomolecules Synthesis, *Chem. Rev.*, 2008, **108**, 3054–3131.

46 Y. Fang, X. Liu, Z. Liu, L. Han, J. Ai, G. Zhao, O. Terasaki, C. Cui, J. Yang, C. Liu, Z. Zhou, L. Chen and S. Che, Synthesis of amino acids by electrocatalytic reduction of CO2 on chiral Cu surfaces, *Chem*, 2023, **9**, 460–471.

47 M. Li, Y. Wu, B.-H. Zhao, C. Cheng, J. Zhao, C. Liu and B. Zhang, Electrosynthesis of amino acids from NO and α-keto acids using two decoupled flow reactors, *Nat. Catal.*, 2023, **6**, 906–915.

48 A. Y. Sukhorukov, Catalytic Reductive Amination of Aldehydes and Ketones With Nitro Compounds: New Light on an Old Reaction, *Front. Chem.*, 2020, **8**, 215.

6942 | *Inorg. Chem. Front.*, 2025, **12**, 6926–6945

This journal is © the Partner Organisations 2025

49 Y. Wu, Z. Jiang, Z. Lin, Y. Liang and H. Wang, Direct electrosynthesis of methylamine from carbon dioxide and nitrate, *Nat. Sustain.*, 2021, **4**, 725–730.

50 C. L. Rooney, Y. Wu, Z. Tao and H. Wang, Electrochemical Reductive N-Methylation with CO2 Enabled by a Molecular Catalyst, *J. Am. Chem. Soc.*, 2021, **143**, 19983–19991.

51 M. Jouny, J.-J. Lv, T. Cheng, B. H. Ko, J.-J. Zhu, W. A. Goddard and F. Jiao, Formation of carbon-nitrogen bonds in carbon monoxide electrolysis, *Nat. Chem.*, 2019, **11**, 846–851.

52 J. Li and N. Kornienko, Electrochemically driven C-N bond formation from CO2 and ammonia at the triple-phase boundary, *Chem. Sci.*, 2022, **13**, 3957–3964.

53 C. Guo, W. Zhou, X. Lan, Y. Wang, T. Li, S. Han, Y. Yu and B. Zhang, Electrochemical Upgrading of Formic Acid to Formamide via Coupling Nitrite Co-Reduction, *J. Am. Chem. Soc.*, 2022, **144**, 16006–16011.

54 C. Chen, N. He and S. Wang, Electrocatalytic C-N Coupling for Urea Synthesis, *Small Sci.*, 2021, **1**, 2100070.

55 X. Song, X. Jin, T. Chen, S. Liu, X. Ma, X. Tan, R. Wang, L. Zhang, X. Tong, Z. Zhao, X. Kang, Q. Zhu, Q. Qian, X. Sun and B. Han, Boosting Urea Electrosynthesis via Asymmetric Oxygen Vacancies in Zn-Doped Fe2O3 Catalysts, *Angew. Chem., Int. Ed.*, 2025, e202501830.

56 C. Lv, L. Zhong, H. Liu, Z. Fang, C. Yan, M. Chen, Y. Kong, C. Lee, D. Liu, S. Li, J. Liu, L. Song, G. Chen, Q. Yan and G. Yu, Selective electrocatalytic synthesis of urea with nitrate and carbon dioxide, *Nat. Sustain.*, 2021, **4**, 868–876.

57 C. Chen, X. Zhu, X. Wen, Y. Zhou, L. Zhou, H. Li, L. Tao, Q. Li, S. Du, T. Liu, D. Yan, C. Xie, Y. Zou, Y. Wang, R. Chen, J. Huo, Y. Li, J. Cheng, H. Su, X. Zhao, W. Cheng, Q. Liu, H. Lin, J. Luo, J. Chen, M. Dong, K. Cheng, C. Li and S. Wang, Coupling N2 and CO2 in H2O to synthesize urea under ambient conditions, *Nat. Chem.*, 2020, **12**, 717–724.

58 L. Xu, X. Tan, Z.-H. He, L. Hao, W. Wang, Z.-T. Liu, A. W. Robertson and Z. Sun, Emerging green catalytic synthesis of biomolecules from CO2 and/or nitrogenous small molecules, *Matter*, 2024, **7**, 59–81.

59 W. Chen, Y. Wu, Y. Jiang, G. Yang, Y. Li, L. Xu, M. Yang, B. Wu, Y. Pan, Y. Xu, Q. Liu, C. Chen, F. Peng, S. Wang and Y. Zou, Catalyst Selection over an Electrochemical Reductive Coupling Reaction toward Direct Electrosynthesis of Oxime from NOx and Aldehyde, *J. Am. Chem. Soc.*, 2024, **146**, 6294–6306.

60 J. Xian, S. Li, H. Su, P. Liao, S. Wang, Y. Zhang, W. Yang, J. Yang, Y. Sun, Y. Jia, Q. Liu, Q. Liu and G. Li, Electrocatalytic Synthesis of Essential Amino Acids from Nitric Oxide Using Atomically Dispersed Fe on N-doped Carbon, *Angew. Chem., Int. Ed.*, 2023, **62**, e202304007.

61 S. Jia, R. Wang, X. Jin, H. Liu, L. Wu, X. Song, L. Zhang, X. Ma, X. Tan, X. Sun and B. Han, In situ Generation of Cyclohexanone Drives Electrocatalytic Upgrading of Phenol to Nylon-6 Precursor, *Angew. Chem., Int. Ed.*, 2024, **63**, e202410972.

62 Y. Liu, X. Tu, X. Wei, D. Wang, X. Zhang, W. Chen, C. Chen and S. Wang, C-Bound or O-Bound Surface: Which One Boosts Electrocatalytic Urea Synthesis?, *Angew. Chem., Int. Ed.*, 2023, **62**, e202300387.

63 X. Tu, X. Zhu, S. Bo, X. Zhang, R. Miao, G. Wen, C. Chen, J. Li, Y. Zhou, Q. Liu, D. Chen, H. Shao, D. Yan, Y. Li, J. Jia and S. Wang, A Universal Approach for Sustainable Urea Synthesis via Intermediate Assembly at the Electrode/Electrolyte Interface, *Angew. Chem., Int. Ed.*, 2024, **63**, e202317087.

64 X. Lu, Z.-C. Yao, X. Ma, Z.-Q. Shi, L. Ding, J. Fu, Z.-H. Lyu, Z. Jiang, S.-Q. Wang, J. Yang, X. Chang, B. Xu and J.-S. Hu, Multiple Secondary Bond-Mediated C-N Coupling over N-Doped Carbon Electrocatalysts, *J. Am. Chem. Soc.*, 2025, **147**, 19342–19352.

65 Y. Zhong, H. Xiong, J. Low, R. Long and Y. Xiong, Recent progress in electrochemical C-N coupling reactions, *eScience*, 2023, **3**, 100086.

66 Z. Xi, H. Hu, Q. Chen, M. Ning, S. Wang, H. Yu, Y. Sun, D.-W. Wang, H. Jin and H.-M. Cheng, 2D Catalysts for Electrocatalytic Nitrate Reduction and C-N Coupling Reactions, *Adv. Funct. Mater.*, 2025, 2425611.

67 C. Zhang, S.-L. Meng, Y.-N. Jing, C. Wang, X.-L. Zhang, H.-X. Wang, C.-H. Tung and L.-Z. Wu, Synergistic C-N Coupling for Efficient Cyclohexanone Oxime Synthesis from Ambient Air by Supported Molecular Catalysts, *Angew. Chem., Int. Ed.*, 2025, **64**, e202506546.

68 X. Sui, L. Wu, S. Jia, X. Jin, X. Sun and B. Han, CO2/NOx-involved Electrochemical C-N Coupling Reactions, *Chem. Res. Chin. Univ.*, 2024, **40**, 764–775.

69 Z. W. Seh, J. Kibsgaard, C. F. Dickens, I. Chorkendorff, J. K. Nørskov and T. F. Jaramillo, Combining theory and experiment in electrocatalysis: Insights into materials design, *Science*, 2017, **355**, eaad4998.

70 Y. Jiao, Y. Zheng, M. Jaroniec and S. Z. Qiao, Design of electrocatalysts for oxygen- and hydrogen-involving energy conversion reactions, *Chem. Soc. Rev.*, 2015, **44**, 2060–2086.

71 S. Nitopi, E. Bertheussen, S. B. Scott, X. Liu, A. K. Engstfeld, S. Horch, B. Seger, I. E. L. Stephens, K. Chan, C. Hahn, J. K. Nørskov, T. F. Jaramillo and I. Chorkendorff, Progress and Perspectives of Electrochemical CO2 Reduction on Copper in Aqueous Electrolyte, *Chem. Rev.*, 2019, **119**, 7610–7672.

72 A. Kulkarni, S. Siahrostami, A. Patel and J. K. Nørskov, Understanding Catalytic Activity Trends in the Oxygen Reduction Reaction, *Chem. Rev.*, 2018, **118**, 2302–2312.

73 M. Xu, H. Zhou, X. Lv, Y. Fang, X. Tu, F. Wang, Q. Han, X. Wang and G. Zheng, Selective Urea Electrosynthesis from CO2 and Nitrate on Spin-Polarized Atomically Ordered PdCuCo, *Adv. Mater.*, 2025, 2505286.

74 Z.-J. Zhao, S. Liu, S. Zha, D. Cheng, F. Studt, G. Henkelman and J. Gong, Theory-guided design of catalytic materials using scaling relationships and reactivity descriptors, *Nat. Rev. Mater.*, 2019, **4**, 792–804.

75 A. D. Handoko, F. Wei, Jenndy, B. S. Yeo and Z. W. Seh, Understanding heterogeneous electrocatalytic carbon

This journal is © the Partner Organisations 2025

Inorg. Chem. Front., 2025, **12**, 6926–6945 | **6943**

dioxide reduction through operando techniques, *Nat. Catal.*, 2018, **1**, 922–934.

76 Y.-H. Wang, X. Jin, M. Xue, M.-F. Cao, F. Xu, G.-X. Lin, J.-B. Le, W.-M. Yang, Z.-L. Yang, Y. Cao, Y. Zhou, W. Cai, Z. Zhang, J. Cheng, W. Guo and J.-F. Li, Characterizing surface-confined interfacial water at graphene surface by in situ Raman spectroscopy, *Joule*, 2023, **7**, 1652–1662.

77 J. H. Montoya, L. C. Seitz, P. Chakthranont, A. Vojvodic, T. F. Jaramillo and J. K. Nørskov, Materials for solar fuels and chemicals, *Nat. Mater.*, 2017, **16**, 70–81.

78 Y. Wu, W. Chen, Y. Jiang, Y. Xu, B. Zhou, L. Xu, C. Xie, M. Yang, M. Qiu, D. Wang, Q. Liu, Q. Liu, S. Wang and Y. Zou, Electrocatalytic Synthesis of Nylon-6 Precursor at Almost 100 % Yield, *Angew. Chem., Int. Ed.*, 2023, **62**, e202305491.

79 J. Wu, L. Xu, Z. Kong, K. Gu, Y. Lu, X. Wu, Y. Zou and S. Wang, Integrated Tandem Electrochemical-chemical-electrochemical Coupling of Biomass and Nitrate to Sustainable Alanine, *Angew. Chem., Int. Ed.*, 2023, **62**, e202311196.

80 Y. Cheng, S. Liu, J. Jiao, M. Zhou, Y. Wang, X. Xing, Z. Chen, X. Sun, Q. Zhu, Q. Qian, C. Wang, H. Liu, Z. Liu, X. Kang and B. Han, Highly Efficient Electrosynthesis of Glycine over an Atomically Dispersed Iron Catalyst, *J. Am. Chem. Soc.*, 2024, **146**, 10084–10092.

81 M. Yuan, J. Chen, Y. Bai, Z. Liu, J. Zhang, T. Zhao, Q. Wang, S. Li, H. He and G. Zhang, Unveiling Electrochemical Urea Synthesis by Co-Activation of CO2 and N2 with Mott-Schottky Heterostructure Catalysts, *Angew. Chem., Int. Ed.*, 2021, **60**, 10910–10918.

82 L. Ni, C. Yu, Q. Wei, D. Liu and J. Qiu, Pickering Emulsion Catalysis: Interfacial Chemistry, Catalyst Design, Challenges, and Perspectives, *Angew. Chem., Int. Ed.*, 2022, **61**, e202115885.

83 X. Zhang, Y. Hou, R. Ettelaie, R. Guan, M. Zhang, Y. Zhang and H. Yang, Pickering Emulsion-Derived Liquid-Solid Hybrid Catalyst for Bridging Homogeneous and Heterogeneous Catalysis, *J. Am. Chem. Soc.*, 2019, **141**, 5220–5230.

84 C. Han, J. Zenner, J. Johny, N. Kaeffer, A. Bordet and W. Leitner, Electrocatalytic hydrogenation of alkenes with Pd/carbon nanotubes at an oil-water interface, *Nat. Catal.*, 2022, **5**, 1110–1119.

85 R. Vácha, S. W. Rick, P. Jungwirth, A. G. F. de Beer, H. B. de Aguiar, J.-S. Samson and S. Roke, The Orientation and Charge of Water at the Hydrophobic Oil Droplet-Water Interface, *J. Am. Chem. Soc*, 2011, 133, 10204–10210.

86 R. Yang, Y. Wang, H. Li, J. Zhou, Z. Gao, C. Liu and B. Zhang, Descriptor-Based Volcano Relations Predict Single Atoms for Hydroxylamine Electrosynthesis, *Angew. Chem., Int. Ed.*, 2024, **63**, e202317167.

87 M. Pera-Titus, L. Leclercq, J.-M. Clacens, F. De Campo and V. Nardello-Rataj, Pickering Interfacial Catalysis for Biphasic Systems: From Emulsion Design to Green Reactions, *Angew. Chem., Int. Ed.*, 2015, **54**, 2006–2021.

88 M. Zhang, R. Ettelaie, T. Li, J. Yang, L. Dong, N. Xue, B. P. Binks, F. Cheng and H. Yang, Pickering emulsion droplets and solid microspheres acting synergistically for continuous-flow cascade reactions, *Nat. Catal.*, 2024, **7**, 295–306.

89 H. Zou, H. Shi, S. Hao, Y. Hao, J. Yang, X. Tian and H. Yang, Boosting Catalytic Selectivity through a Precise Spatial Control of Catalysts at Pickering Droplet Interfaces, *J. Am. Chem. Soc.*, 2023, **145**, 2511–2522.

90 Y. Wang, C. Wang, M. Li, Y. Yu and B. Zhang, Nitrate electroreduction: mechanism insight, in situ characterization, performance evaluation, and challenges, *Chem. Soc. Rev.*, 2021, **50**, 6720–6733.

91 D. C. Cantu, A. B. Padmaperuma, M.-T. Nguyen, S. A. Akhade, Y. Yoon, Y.-G. Wang, M.-S. Lee, V.-A. Glezakou, R. Rousseau and M. A. Lilga, Erratum to "A Combined Experimental and Theoretical Study on the Activity and Selectivity of the Electrocatalytic Hydrogenation of Aldehydes", *ACS Catal.*, 2019, **9**, 1738–1738.

92 M. Cocivera and A. Effio, Flow nuclear magnetic resonance study of the rapid addition of hydroxylamine to acetone and the rate-determining dehydration of the carbinolamine, *J. Am. Chem. Soc.*, 1976, **98**, 7371–7374.

93 Y. Pan, C. Zhang, Z. Liu, C. Chen and Y. Li, Structural Regulation with Atomic-Level Precision: From Single-Atomic Site to Diatomic and Atomic Interface Catalysis, *Matter*, 2020, **2**, 78–110.

94 X. Wei, Y. Liu, X. Zhu, S. Bo, L. Xiao, C. Chen, T. T. T. Nga, Y. He, M. Qiu, C. Xie, D. Wang, Q. Liu, F. Dong, C.-L. Dong, X.-Z. Fu and S. Wang, Dynamic Reconstitution Between Copper Single Atoms and Clusters for Electrocatalytic Urea Synthesis, *Adv. Mater.*, 2023, **35**, 2300020.

95 Y. Sheng, J. Xie, R. Yang, H. Yu, K. Deng, J. Wang, H. Wang, L. Wang and Y. Xu, Modulating Hydrogen Adsorption by Unconventional p-d Orbital Hybridization over Porous High-Entropy Alloy Metallene for Efficient Electrosynthesis of Nylon-6 Precursor, *Angew. Chem., Int. Ed.*, 2024, **63**, e202410442.

96 L. Zhang, J. Feng, S. Liu, X. Tan, L. Wu, S. Jia, L. Xu, X. Ma, X. Song, J. Ma, X. Sun and B. Han, Atomically Dispersed Ni-Cu Catalysts for pH-Universal CO2 Electroreduction, *Adv. Mater.*, 2023, **35**, 2209590.

97 P. Liao, B. Zeng, S. Li, Y. Zhang, R. Xiang, J. Kang, Q. Liu and G. Li, Cu-Bi Bimetallic Catalysts Derived from Metal-Organic Framework Arrays on Copper Foam for Efficient Glycine Electrosynthesis, *Angew. Chem., Int. Ed.*, 2025, **64**, e202417130.

98 M. He, Y. Wu, R. Li, Y. Wang, C. Liu and B. Zhang, Aqueous pulsed electrochemistry promotes C-N bond formation via a one-pot cascade approach, *Nat. Commun.*, 2023, **14**, 5088.

99 Y. Fan, T. Liu, Y. Yan, Z. Xia, Y. Lu, Y. Pan, R. Wang, D. Xie, Z. Zhu, T. T. T. Nga, C.-L. Dong, Y. Jing, Y. Li, S. Wang and Y. Zou, Electrochemical synthesis of formamide by C-N coupling with amine and CO2 with a high faradaic efficiency of 37.5%, *Chem*, 2024, **10**, 2437–2449.

6944 | *Inorg. Chem. Front.*, 2025, **12**, 6926–6945

This journal is © the Partner Organisations 2025

100 Y. Pan, Y. Zou, C. Ma, T. T. T. Nga, Q. An, R. Miao, Z. Xia, Y. Fan, C.-L. Dong, Q. Liu and S. Wang, Electrocatalytic Coupling of Nitrate and Formaldehyde for Hexamethylenetetramine Synthesis via C-N Bond Construction and Ring Formation, *J. Am. Chem. Soc.*, 2024, **146**, 19572–19579.

101 Y. Wang, X. Zhu, Q. An, X. Zhang, X. Wei, C. Chen, H. Li, D. Chen, Y. Zhou, Q. Liu, H. Shao and S. Wang, Electron Deficiency is More Important than Conductivity in C-N Coupling for Electrocatalytic Urea Synthesis, *Angew. Chem., Int. Ed.*, 2024, **63**, e202410938.

102 X. Wei, X. Wen, Y. Liu, C. Chen, C. Xie, D. Wang, M. Qiu, N. He, P. Zhou, W. Chen, J. Cheng, H. Lin, J. Jia, X.-Z. Fu and S. Wang, Oxygen Vacancy-Mediated Selective C-N Coupling toward Electrocatalytic Urea Synthesis, *J. Am. Chem. Soc.*, 2022, **144**, 11530–11535.

103 X. Zhang, X. Zhu, S. Bo, C. Chen, Q. Zhai, S. Li, X. Tu, J. Zheng, D. Wang, X. Wei, W. Chen, T. Wang, Y. Li, Q. Liu, S. P. Jiang, L. Dai and S. Wang, Selective nitrogen fixation via Janus C-N coupling in co-electrolysis, *Chem*, 2024, **10**, 1516–1527.

104 S. Jia, X. Tan, L. Wu, Z. Zhao, X. Song, J. Feng, L. Zhang, X. Ma, Z. Zhang, X. Sun and B. Han, Lignin-derived carbon nanosheets boost electrochemical reductive amination of pyruvate to alanine, *iScience*, 2023, **26**, 107776.

105 R. Xiang, S. Wang, P. Liao, F. Xie, J. Kang, S. Li, J. Xian, L. Guo and G. Li, Electrocatalytic Synthesis of Pyridine Oximes using in Situ Generated NH$_2$OH from NO species on Nanofiber Membranes Derived from NH2-MIL-53(Al), *Angew. Chem., Int. Ed.*, 2023, **62**, e202312239.

106 S. Wang, R. Xiang, P. Liao, J. Kang, S. Li, M. Mao, L. Liu and G. Li, Highly Efficient One-pot Electrosynthesis of Oxime Ethers from NOx over Ultrafine MgO Nanoparticles Derived from Mg-based Metal-Organic Frameworks, *Angew. Chem., Int. Ed.*, 2024, **63**, e202405553.

107 Z. Zhu, Y. Jiang, L. Xu, Q. An, T. T. T. Nga, J. Chen, Y. Fan, Q. Liu, C.-L. Dong, S. Wang and Y. Zou, Highly Efficient Synthesis of α-Amino Acids via Electrocatalytic C-N Coupling Reaction Over an Atomically Dispersed Iron Loaded Defective TiO2, *Adv. Mater.*, 2025, **37**, 2409864.

108 H. Li, L. Xu, S. Bo, Y. Wang, H. Xu, C. Chen, R. Miao, D. Chen, K. Zhang, Q. Liu, J. Shen, H. Shao, J. Jia and S. Wang, Ligand engineering towards electrocatalytic urea synthesis on a molecular catalyst, *Nat. Commun.*, 2024, **15**, 8858.

109 R. Shi, X. Zhang, C. Li, Y. Zhao, R. Li, G. I. N. Waterhouse and T. Zhang, Electrochemical oxidation of concentrated benzyl alcohol to high-purity benzaldehyde via superwetting organic-solid-water interfaces, *Sci. Adv.*, 2024, **10**, eadn0947.

110 J. Shao, N. Meng, Y. Wang, B. Zhang, K. Yang, C. Liu, Y. Yu and B. Zhang, Scalable Electrosynthesis of Formamide through C-N Coupling at the Industrially Relevant Current Density of 120 mA cm-2, *Angew. Chem., Int. Ed.*, 2022, **61**, e202213009.

111 N. Meng, J. Shao, H. Li, Y. Wang, X. Fu, C. Liu, Y. Yu and B. Zhang, Electrosynthesis of formamide from methanol and ammonia under ambient conditions, *Nat. Commun.*, 2022, **13**, 5452.

112 J. Xian, S. Li, H. Su, P. Liao, S. Wang, R. Xiang, Y. Zhang, Q. Liu and G. Li, Electrosynthesis of α-Amino Acids from NO and other NOx species over CoFe alloy-decorated Self-standing Carbon Fiber Membranes, *Angew. Chem., Int. Ed.*, 2023, **62**, e202306726.

113 X. Zhang, X. Zhu, S. Bo, C. Chen, K. Cheng, J. Zheng, S. Li, X. Tu, W. Chen, C. Xie, X. Wei, D. Wang, Y. Liu, P. Chen, S. P. Jiang, Y. Li, Q. Liu, C. Li and S. Wang, Electrocatalytic Urea Synthesis with 63.5 % Faradaic Efficiency and 100 % N-Selectivity via One-step C-N coupling, *Angew. Chem., Int. Ed.*, 2023, **62**, e202305447.

114 X. Zhang, X. Zhu, S. Bo, C. Chen, M. Qiu, X. Wei, N. He, C. Xie, W. Chen, J. Zheng, P. Chen, S. P. Jiang, Y. Li, Q. Liu and S. Wang, Identifying and tailoring C-N coupling site for efficient urea synthesis over diatomic Fe-Ni catalyst, *Nat. Commun.*, 2022, **13**, 5337.

This journal is © the Partner Organisations 2025

Inorg. Chem. Front., 2025, **12**, 6926–6945 | **6945**